

# LoBoost : Fast Model-Native Local Conformal Prediction for Gradient-Boosted Trees

Vagner Silva Santos<sup>1,2</sup>, Victor Coscrato<sup>1</sup>, Luben M. C. Cabezas<sup>1,2,3</sup>,  
Rafael Izbicki<sup>1</sup>, and Thiago R. Ramos<sup>1</sup>

<sup>1</sup> Department of Statistics, Federal University of São Carlos, São Carlos, São Paulo, Brazil

<sup>2</sup> Institute of Mathematics and Computer Science, University of São Paulo, São Carlos, São Paulo, Brazil

<sup>3</sup> Université Grenoble Alpes, Inria, CNRS, Grenoble INP, LJK, France

February 27, 2026

Gradient-boosted decision trees are among the strongest off-the-shelf predictors for tabular regression, but point predictions alone do not quantify uncertainty. Conformal prediction provides distribution-free marginal coverage, yet split conformal uses a single global residual quantile and can be poorly adaptive under heteroscedasticity. Methods that improve adaptivity typically fit auxiliary nuisance models or introduce additional data splits/partitions to learn the conformal score, increasing cost and reducing data efficiency. We propose **LoBoost**, a model-native local conformal method that reuses the fitted ensemble’s leaf structure to define multiscale calibration groups. Each input is encoded by its sequence of visited leaves; at resolution level  $k$ , we group points by matching prefixes of leaf indices across the first  $k$  trees and calibrate residual quantiles within each group. **LoBoost** requires no retraining, auxiliary models, or extra splitting beyond the standard train/calibration split. Experiments show competitive interval quality, improved test MSE on most datasets, and large calibration speedups.

## 1. Introduction

Gradient-boosted decision trees are among the strongest off-the-shelf predictors for tabular regression (Friedman, 2001; Chen and Guestrin, 2016; Grinsztajn et al., 2022). In many applications, however, accurate point predictions are not enough: unobserved covariates, measurement noise, and intrinsic randomness make the response uncertain. Practitioners therefore need prediction intervals that adapt to each input and quantify uncertainty reliably.

Conformal prediction (CP) offers a simple and rigorous route to uncertainty quantification. Given any predictor  $g$  and an i.i.d. calibration set, split conformal constructs intervals  $C(X)$  with finite-sample, distribution-free marginal coverage,  $\mathbb{P}(Y \in C(X)) \geq 1 - \alpha$ , under exchangeability (Vovk et al., 2005; Shafer and Vovk, 2008; Angelopoulos et al., 2023; Zhou et al., 2025). In regression, the resulting interval width is controlled by an empirical quantile of calibration residuals. Classical split conformal uses a single global residual quantile, which can yield overly wide intervals in low-noise regions and insufficient adaptivity under heteroscedasticity (Lei et al., 2018; Guan, 2023).

A natural remedy is *partition-based* (or local) conformal prediction: estimate separate residual quantiles within regions  $A \subseteq \mathcal{X}$  and obtain coverage conditional on  $X \in A$ . The practical challenge is choosing these regions: they must be small enough that residuals are approximately homogeneous, yet large enough to contain enough calibration points for stable quantile estimation. Recent work addresses this trade-off by learning data-driven partitions with auxiliary trees or by defining soft neighborhoods in feature space (Boström and Johansson, 2020; Guan, 2023; Martinez et al., 2024; Fröhlich et al., 2025; Cabezas et al., 2025b). A different line of work induces adaptivity by modifying the nonconformity score using additional nuisance estimates, such as conditional scales or quantiles (Lei et al., 2018; Romano et al., 2019; Cabezas et al., 2025c; Izbicki et al., 2020, 2022; Dheur et al., 2024).

While effective, local conformal methods introduce additional estimation beyond the base regressor—learning an auxiliary partition or nuisance functions, or using extra splitting/cross-fitting—reducing data efficiency. For gradient-boosted trees, this overlooks a key fact: the trained ensemble already induces a rich, nested partition of  $\mathcal{X}$  via its leaf structure. We introduce `LoBoost`, which reuses this model-induced partition to calibrate residual quantiles locally. Concretely, we represent each input  $x$  by the sequence of leaves it visits along the ensemble,  $\mathbf{L}_T(x) = (L_1(x), \dots, L_T(x))$ , and define a local region around  $x$  by requiring agreement on the first  $k$  trees, i.e., matching the prefix  $(L_1(x), \dots, L_k(x))$ . This yields a nested, multiscale partition—coarse when  $k$  is small, increasingly refined as  $k$  grows—on which we calibrate residual quantiles.

We then perform split conformal calibration within these regions—retaining finite-sample marginal validity by construction while adapting interval widths to local residual distributions—without retraining the predictor or fitting additional functions. This leads to improved predictive power of the base model, while keeping local validity of the prediction sets.

Figure 1 illustrates the motivation for `LoBoost` on the heteroscedastic 1D simulation (Supplementary Material A.4): `LoBoost` produces locally adaptive intervals (narrow in low-noise regions, wide in high-noise regions) and attains conditional coverage closer to the nominal  $1 - \alpha = 0.9$  than standard split conformal/ICP.

## Contributions.

- **Model-native local conformal prediction for boosted trees.** We use leaf-index prefixes from the fitted boosted ensemble to define a multiscale partition of  $\mathcal{X}$  and perform conformal calibration within these cells, preserving finite-sample marginal validity and yielding locally adaptive intervals. Empirically, our interval quality is

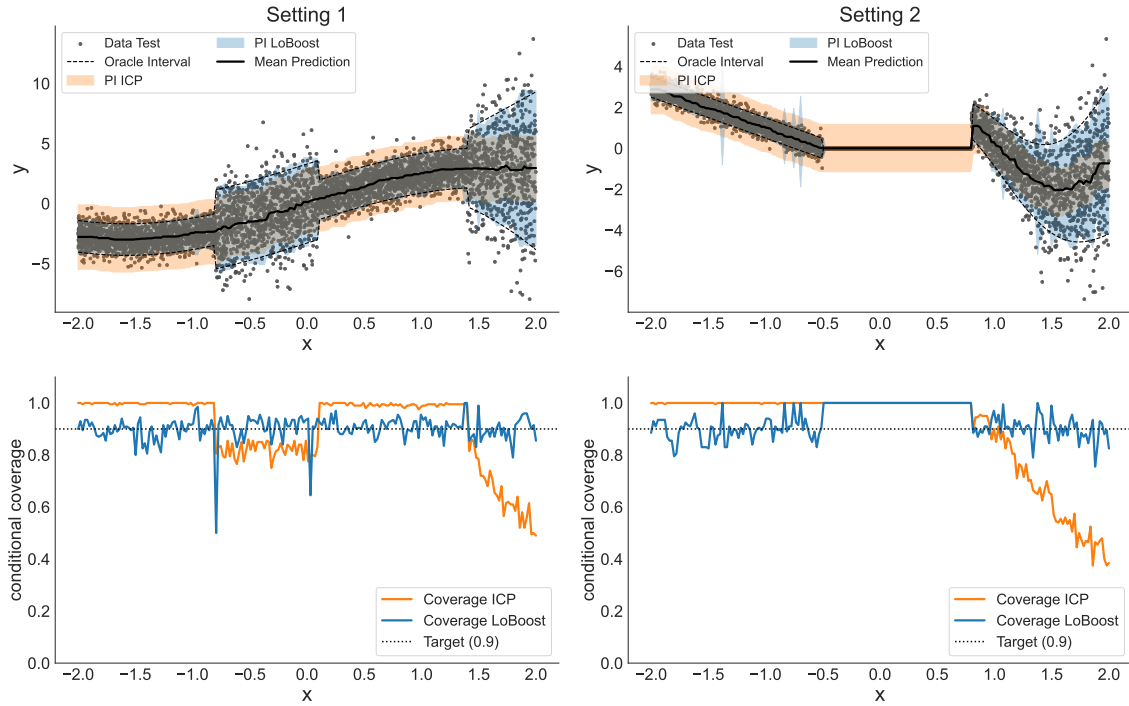


Figure 1: Comparison of prediction intervals and conditional coverage for **LoBoost** and **ICP** on two synthetic mechanisms. Top: estimated intervals with the oracle interval and test data—**LoBoost** tracks the oracle more closely, handling heteroscedasticity and discontinuities better than **ICP**. Bottom: empirical conditional coverage across the feature space (target  $1 - \alpha = 0.9$ )—**LoBoost** stays near 0.9, while **ICP** deviates, reflecting **LoBoost**'s meaningful feature-space partitions.

competitive with the strongest *competing* local baseline, with SMIS efficiency ranging from 77.8% to 99.6% across datasets.

- **Data efficiency and simplicity.** **LoBoost** requires no auxiliary partition model, no retraining of the base learner, and no extra data splitting beyond standard train/calibration split. This in turn yields better predictive power, while still having local coverage guarantees: we outperform the best-SMIS baseline in point accuracy on 10/11 datasets, with test MSE improvements typically around 3–4% and reaching about 5–6% in the best case.
- **Theory connecting boosting stability to approximate conditional coverage.** Under mild decay/stability conditions on later boosting updates, we show residuals are approximately homogeneous within boosting-induced cells, implying asymptotic conditional validity while retaining finite-sample guarantees.
- **Practical gains in calibration time.** Reusing the model-induced partition yields substantial computational savings: relative to the best-SMIS method, **LoBoost** is faster on 9/11 datasets, with median speedup  $17\times$  and up to  $126\times$ .

## 1.1. Relation to Other Work

**Uncertainty quantification for boosted models (non-conformal).** Recent approaches for endowing boosting with uncertainty quantification generally fall into two categories. First,

probabilistic frameworks like NGBoost (Duan et al., 2020) and PGBM (Sprangers et al., 2021) assume a conditional parametric distribution, optimizing its parameters via natural gradients to minimize a proper scoring rule. Second, statistical inference methods, such as the work by Fang et al. (2025), rely on Central Limit Theorems to construct intervals based on the asymptotic normality of the boosted estimator. However, both strategies lack the rigorous finite-sample, distribution-free validity of conformal prediction, relying instead on specific parametric forms or asymptotic approximations that may not hold in practice. Thus, these methods are model-native but not distribution-free; `LoBoost` instead is both model-native and distribution-free.

**Conformal prediction with boosting as a base learner.** Conformal prediction provides finite-sample, distribution-free coverage for any underlying regressor, including boosted trees. Most existing work uses boosting primarily as a strong black-box predictor inside conformal wrappers (e.g., CQR-style efficiency gains, residual scoring, or distributional regression) (Romano et al., 2019; Chernozhukov et al., 2021; Xu et al., 2024; Lai et al., 2025). In contrast, we leverage the *internal* structure of the boosted ensemble—its sequence of tree partitions—to define locality for calibration. This avoids extra data splitting, and therefore improved predictive power, while keeping the distribution-free guarantees. In a different approach, Xie et al. (2024) propose Boosted CP Intervals, a post-hoc method that boosts a conformity score to improve interval length or conditional coverage. Unlike our approach, which uses leaf-based partitions of the boosted tree for local calibration, theirs learns a new score from model outputs without using the tree structure.

**Local and partition-based conformal prediction.** Exact conditional coverage is generally impossible without strong assumptions, motivating local or group-conditional targets (Lei and Wasserman, 2014; Vovk, 2012; Foygel Barber et al., 2021; Lei et al., 2018; Izbicki, 2025). Local CP has been studied via kernel/neighborhood weighting (Guan, 2023), multivald/group-conditional optimization (Jung et al., 2023; Kiyani et al., 2024), and Mondrian-style partitions (Vovk et al., 2005; Boström and Johansson, 2020). Recently, tree-based variants were employed to learn residual-driven partitions using auxiliary trees trained on a calibration set (Martinez et al., 2024; Cabezas et al., 2025b,d,a). In contrast, we reuse the base model’s internal tree-induced codes to define groups, requiring no auxiliary partition estimator. This leads to improved predictive power of the base boosting model.

## 2. Background

We consider a dataset of size  $n$ , denoted by  $\mathcal{D} = \{(X_i, Y_i)\}_{i=1}^n$ , where the pairs  $(X_i, Y_i)$  are independent and identically distributed according to a joint distribution  $P$ , with  $(X_i, Y_i) \in \mathcal{X} \times \mathcal{Y}$ . We assume that  $\mathcal{D}$  is partitioned into a training set  $\mathcal{D}_{\text{train}}$  and a calibration set  $\mathcal{D}_{\text{cal}}$ , with respective sizes  $|\mathcal{D}_{\text{train}}| = n_{\text{train}}$  and  $|\mathcal{D}_{\text{cal}}| = n_{\text{cal}}$ .

## 2.1. Conformal Prediction

Conformal prediction constructs prediction sets with finite-sample coverage under exchangeability (Vovk et al., 2005). We focus on *split conformal*: train a regressor  $g$  on  $\mathcal{D}_{\text{train}}$  and calibrate on  $\mathcal{D}_{\text{cal}} = \{(X_j, Y_j)\}_{j=1}^{n_{\text{cal}}}$  using a nonconformity score  $s(x, y)$ . Define calibration scores  $S_j := s(X_j, Y_j)$ ,  $j = 1, \dots, n_{\text{cal}}$ . Let  $S_{(1)} \leq \dots \leq S_{(n_{\text{cal}})}$  be the sorted scores and set  $\hat{q}_{1-\alpha} := S_{(\lceil (n_{\text{cal}}+1)(1-\alpha) \rceil)}$ , the  $(1-\alpha)(1+1/n_{\text{cal}})$  empirical quantile. The split-conformal prediction set is

$$C(x) := \{y \in \mathcal{Y} : s(x, y) \leq \hat{q}_{1-\alpha}\}.$$

Under exchangeability of the calibration data and an independent test pair  $(X, Y)$ ,

$$\mathbb{P}(Y \in C(X)) \geq 1 - \alpha.$$

In regression, we use the absolute-residual score  $s(x, y) = |y - g(x)|$ , yielding the interval  $C(x) = [g(x) - \hat{q}_{1-\alpha}, g(x) + \hat{q}_{1-\alpha}]$ .

**Partition-based conformal.** To obtain locally adaptive thresholds (Lei et al., 2018), let  $\mathcal{A} = \{A_1, \dots, A_K\}$  be a partition of  $\mathcal{X}$  (determined without using calibration responses). For each cell  $A \in \mathcal{A}$ , let

$$J_A := \{j : X_j \in A\} \text{ and } m_A := |J_A|.$$

Define the within-cell quantile  $\hat{q}_{A,1-\alpha}$  as the  $(1-\alpha)(1+\frac{1}{m_A})$  empirical quantile of  $\{S_j : j \in J_A\}$ . Then set  $\hat{q}_{1-\alpha}(x) = \hat{q}_{A,1-\alpha}$  for the unique  $A$  with  $x \in A$ , and define  $C(x) := \{y : s(x, y) \leq \hat{q}_{1-\alpha}(x)\}$ . Under exchangeability, for every cell  $A$ ,

$$\mathbb{P}(Y \in C(X) \mid X \in A) \geq 1 - \alpha.$$

With  $s(x, y) = |y - g(x)|$ , this gives piecewise-constant local intervals  $[g(x) \pm \hat{q}_{1-\alpha}(x)]$ .

## 2.2. Gradient Boosting

Gradient boosting can be interpreted as (approximate) *functional gradient descent* on a risk functional (Friedman, 2001; Grubb and Bagnell, 2012). We present the squared-loss view, which is enough to motivate the sequential, coarse-to-fine structure we exploit later.

Let  $(X, Y) \sim P$ , with  $X \in \mathcal{X}$  and  $Y \in \mathbb{R}$ . Consider the squared-risk functional

$$\mathcal{L}(g) := \frac{1}{2} \mathbb{E} [(Y - g(X))^2].$$

A standard calculation yields the functional gradient

$$-\nabla \mathcal{L}(g)(x) = \mathbb{E}[Y - g(X) \mid X = x],$$

so the negative gradient corresponds to the (population) regression residual.

Boosting builds an additive predictor by iteratively fitting a weak learner to the current residuals. Let  $\mathcal{H}$  denote the weak learner class, in our case, regression trees. Given training

data  $\{(x_i, y_i)\}_{i=1}^n$  and a current predictor  $g_{t-1}$ , define residuals  $u_i^{(t)} := y_i - g_{t-1}(x_i)$  and fit

$$h_t \in \arg \min_{h \in \mathcal{H}} \frac{1}{n} \sum_{i=1}^n (u_i^{(t)} - h(x_i))^2.$$

The model is then updated by the standard gradient-boosting additive step

$$g_t(x) = g_{t-1}(x) + \eta h_t(x), \quad t = 1, \dots, T,$$

starting from an initial predictor  $g_0$  (e.g., a constant). Unrolling the recursion yields the usual additive form

$$g_T(x) = g_0(x) + \sum_{t=1}^T \eta h_t(x), \quad h_t \in \mathcal{H}, \quad (1)$$

i.e., a sequence of progressively refined corrections. Because each new tree is trained on the *remaining* residual signal, boosting behaves like a descent procedure: as iterations proceed, the residuals typically shrink, so later trees act as smaller corrective refinements (especially under shrinkage  $\eta$ ). This coarse-to-fine behavior is the key intuition behind defining multiscale regions using *prefixes* of boosting paths in Section 3.

### 3. Our Method: LoBoost

Next, we describe how the internal structure of a gradient-boosted ensemble can be leveraged to construct partition-based conformal predictors.

#### 3.1. Boosting-Induced Partitions

The sequential nature of gradient boosting induces a hierarchical organization of the feature space: early trees capture coarse, global structure, while later trees introduce progressively finer refinements. As a result, the boosting procedure naturally defines a multiscale, nested decomposition of the feature space. This viewpoint is inspired by earlier work on task-specific similarity learning and boosting-based blocking schemes (Shakhnarovich, 2005; Ramos et al., 2024).

Let  $L_t(x)$  denote the leaf index reached by a point  $x \in \mathcal{X}$  in the  $t$ -th regression tree  $h_t$ , as defined in (1). The boosted ensemble therefore associates each input with a sequence of leaf identifiers,

$$\mathbf{L}_T(x) = (L_1(x), L_2(x), \dots, L_T(x)),$$

which provides a hierarchical encoding of the feature space induced by the boosting trajectory. Specifically, for a resolution level  $k \leq T$ , we say that two points  $x$  and  $x'$  belong to the same region at depth  $k$  if they agree on the first  $k$  entries of this encoding:

$$x \sim_k x' \iff L_t(x) = L_t(x') \text{ for all } t \leq k.$$

We denote by

$$\mathcal{R}_k(x) = \{x' \in \mathcal{X} : x' \sim_k x\},$$

the equivalence class of  $x$  at depth  $k$ , which we refer to as a *boosting-induced region*.

Within any region  $\mathcal{R}_k(x)$ , all points follow the same sequence of leaf decisions for the first  $k$  boosting iterations. As a consequence, any variation of the predictor  $g_T$  across such a region can only arise from the contributions of the remaining trees  $t > k$ . This observation suggests that, as the influence of later trees diminishes, boosting-induced regions should exhibit increasing local regularity. We now make this intuition precise:

**Proposition 1** (Continuity of Gradient Boosting). *Fix  $x \in \mathcal{X}$ . For any  $\varepsilon > 0$  and any  $k \leq T$ , we have*

$$\mathbb{P}(|g_T(X) - g_T(x)| \geq \varepsilon \mid X \in \mathcal{R}_k(x)) \leq \Lambda(x, k, \varepsilon),$$

where we write:

$$\Lambda \equiv \Lambda(x, k, \varepsilon) = \frac{\eta^2(T-k)}{\varepsilon^2} \sum_{t=k+1}^T \mathbb{E} \left[ (h_t(X) - h_t(x))^2 \mid X \in \mathcal{R}_k(x) \right].$$

Proposition 1 shows that the variability of the boosted predictor within a boosting-induced region  $\mathcal{R}_k(x)$  is controlled by the cumulative contribution of the trees added after depth  $k$ . In particular, continuity follows whenever the influence of these later trees decreases sufficiently fast with  $t$ .

To obtain a tractable sufficient condition for this behavior, we assume that the within-region variability of later trees decays geometrically.

**Assumption 1** (Second moment decay). *Fix  $x \in \mathcal{X}$ . There exist constants  $C(x) > 0$  and  $\rho \in (0, 1)$  such that for all  $k \leq T$  and all  $t > k$ ,*

$$\mathbb{E} [(h_t(X) - h_t(x))^2 \mid X \in \mathcal{R}_k(x)] \leq C(x) \rho^t.$$

Assumption 1 is motivated by the gradient-descent view of boosting: as the ensemble approaches the regression function, the magnitude of later updates should decay. We adopt it as a convenient stability condition that yields an explicit rate. Indeed, let  $g_*(x) = \mathbb{E}[Y \mid X = x]$ . For squared loss, the negative functional gradient is

$$-\nabla \mathcal{L}(g_t)(x) = g_*(x) - g_t(x).$$

In the idealized population setting, exact gradient descent with step size  $\eta \in (0, 1)$  gives

$$g_{t+1}(x) = g_t(x) + \eta(g_*(x) - g_t(x)),$$

and subtracting  $g_*(x)$  from both sides yields

$$\nabla \mathcal{L}(g_{t+1}) = (1 - \eta) \nabla \mathcal{L}(g_t),$$

so the residual contracts geometrically with  $t$ . Additional empirical support is provided in Supplementary Material D.

In practice, boosting replaces the exact gradient step by fitting a weak learner to residuals; under a standard *edge* condition, the fitted learner achieves non-negligible alignment with the population negative gradient (Grubb and Bagnell, 2012). This supports the in-

tuition that the residual signal decreases along the boosting iterations, so later trees are typically fitted to smaller-magnitude residuals. It is therefore natural to expect the size of the updates  $h_t$  to decrease with  $t$ , motivating the geometric decay postulated in Assumption 1. The following corollary makes this simplification explicit.

**Corollary 1.** *Under Assumption 1, the quantity  $\Lambda$  in Proposition 1 satisfies*

$$\Lambda \leq \frac{C(x)\eta^2(T-k)}{\varepsilon^2(1-\rho)}\rho^{k+1}.$$

In words, points that share the same boosting path up to depth  $k$  exhibit nearly identical predictions.

### 3.2. Local Conformal Prediction with Boosted Partitions

We present our method for local split-conformal predictor based on the boosting-induced regions  $\mathcal{R}_k(x)$ .

Let  $\mathcal{D}_{\text{train}}$  and  $\mathcal{D}_{\text{cal}}$  denote the training and calibration sets, respectively, and let  $g_T$  be the gradient boosting predictor trained on  $\mathcal{D}_{\text{train}}$ . Fix a resolution level  $k$  and consider a test point  $x \in \mathcal{X}$ . Local conformal prediction is then obtained by calibrating within the region  $\mathcal{R}_k(x)$ , as described below.

1. **Region identification.** Fix a resolution level  $k \leq T$  and identify the boosting-induced region containing  $x$ ,

$$\mathcal{R}_k(x) = \{x' \in \mathcal{X} : x' \sim_k x\}.$$

2. **Local calibration.** Using the calibration set  $\mathcal{D}_{\text{cal}} = \{(X_j, Y_j)\}_{j=1}^{n_{\text{cal}}}$ , compute the nonconformity scores

$$S_j = s(X_j, Y_j) = |Y_j - g_T(X_j)|, j = 1, \dots, n_{\text{cal}},$$

and collect the indices of calibration points that fall in the same region as  $x$ ,

$$J_k(x) := \{j : X_j \in \mathcal{R}_k(x)\}, m_k(x) := |J_k(x)|.$$

3. **Local quantile estimation.** Let  $\hat{q}_{k,1-\alpha}(x)$  be the  $(1-\alpha)(1+1/m_k(x))$ -empirical quantile of  $\{S_j : j \in J_k(x)\}$ .

This yields the local split-conformal interval at resolution  $k$ ,

$$\hat{C}_k(x) = [g_T(x) - \hat{q}_{k,1-\alpha}(x), g_T(x) + \hat{q}_{k,1-\alpha}(x)].$$

**Theorem 1** (Local coverage). *Fix a resolution level  $k$  and a point  $x \in \mathcal{X}$ . Suppose that the calibration pairs  $\{(X_i, Y_i) : X_i \in \mathcal{R}_k(x)\}$  and the test pair  $(X, Y)$  are exchangeable. Let  $\hat{C}_k(\cdot)$  denote the local conformal prediction interval constructed above. Then*

$$\mathbb{P}\left(Y \in \hat{C}_k(X) \mid X \in \mathcal{R}_k(x)\right) \geq 1 - \alpha.$$

Moreover, if ties among the local calibration scores occur with probability zero, then

$$\mathbb{P}\left(Y \in \widehat{C}_k(X) \mid X \in \mathcal{R}_k(x)\right) \leq 1 - \alpha + \frac{1}{m_k(x) + 1}.$$

Theorem 1 establishes a finite-sample coverage guarantee within each boosting-induced region  $\mathcal{R}_k(x)$ . As in standard partition-based conformal prediction, the sharpness of this guarantee depends critically on the number of calibration points available within the region. In particular, accurate estimation of the local quantile  $\widehat{q}_{k,1-\alpha}(x)$  requires that  $\mathcal{R}_k(x)$  contain a sufficient number of calibration samples. However, since boosting-induced partitions become increasingly fine as  $k$  grows, some regions may be too sparse to support reliable calibration. We address this issue in Section 4.

As shown in the previous section, the partitions  $\mathcal{R}_k(x)$  enjoy a stability property: for moderately large  $k$ , the predictor  $g_T$  varies little within each  $\mathcal{R}_k(x)$ . This local regularity enables local conformal calibration:

**Corollary 2** (Local behavior of the residual). *Let  $s(x, y) := |y - g_T(x)|$ . For any  $\varepsilon > 0$  and any  $x$ ,*

$$\mathbb{P}\left(|s(X, Y) - s(x, Y)| \geq \varepsilon \mid X \in \mathcal{R}_k(x)\right) \leq \Lambda(x, k, \varepsilon).$$

Moreover, under Assumption 1 and Corollary 1, for any  $\delta \in (0, 1)$ , if

$$k \geq \frac{1}{-\log \rho} \log \left( \frac{C(x) \eta^2 T}{\delta \varepsilon^2 (1 - \rho)} \right),$$

then  $\Lambda(x, k, \varepsilon) \leq \delta$ .

Corollary 2 shows that, for a logarithmic choice of the resolution level  $k$ , residual scores are approximately homogeneous within each boosting-induced region  $\mathcal{R}_k(x)$ . In particular, conditional on  $X \in \mathcal{R}_k(x)$ , the distribution of  $s(X, Y) = |Y - g_T(X)|$  behaves approximately like the pointwise score  $s(x, Y)$ . Intuitively, for any  $t \geq 0$ ,

$$\mathbb{P}(s(X, Y) \leq t \mid X \in \mathcal{R}_k(x)) \approx \mathbb{P}(s(x, Y) \leq t \mid X = x).$$

This local homogeneity both motivates our partition-based method and provides the main stepping stone for establishing asymptotic conditional coverage.

### 3.3. Asymptotic Conditional Coverage

The local guarantee in Theorem 1 controls coverage conditional on the event  $\{X \in \mathcal{R}_k(x)\}$ . A natural question is whether, as the boosting resolution increases, this can be strengthened to coverage conditional on the point event  $\{X = x\}$ . Such a strengthening is delicate: without additional structure, distribution-free conditional coverage uniformly over  $x$  is impossible except for trivial prediction sets (Vovk, 2012; Foygel Barber et al., 2021; Lei et al., 2018).

Our model provides a natural route to this strengthening. The key boosting-specific ingredient is residual homogeneity inside  $\mathcal{R}_k(x)$ . Corollary 2 implies that, for sufficiently large  $k$ , the residual at a random  $X \in \mathcal{R}_k(x)$  is close to the residual at the fixed point  $x$  with high probability.

Combined with Assumptions 3–4 (which ensure that conditioning on  $\mathcal{R}_k(x)$  approaches conditioning on  $x$  as the regions shrink) and Assumption 2 (which ensures consistent estimation of local conformal quantiles), this yields asymptotic conditional coverage at  $x$ . We defer all assumptions and proofs to the Supplementary Material E.

**Theorem 2** (Asymptotic conditional coverage). *Fix  $\alpha \in (0, 1)$  and  $x \in \mathcal{X}$ . Let  $\widehat{C}_k(x)$  be the local split-conformal interval constructed at resolution  $k$  using calibration residuals restricted to  $\mathcal{R}_k(x)$ . Assume Assumptions 1, 2, 3, and 4, and assume that the conditional residual distribution function  $\mathbb{P}(|Y - g_T(x)| \leq t \mid X = x)$  is continuous. Let  $k(T) := \left\lceil \frac{2}{-\log \rho} \log T \right\rceil$ . Then the corresponding local split-conformal interval satisfies*

$$\lim_{T \rightarrow \infty} \mathbb{P}\left(Y \in \widehat{C}_{k(T)}(x) \mid X = x\right) = 1 - \alpha.$$

In words, under the stated regularity and local sample size conditions, **LoBoost** achieves the desired conditional coverage at  $x$  asymptotically.

## 4. Resolution Selection and Aggregation

The theoretical results in Section 3.1 motivate boosting-induced partitions for local conformal calibration, but practical use requires controlling the resolution level  $k$  and finite-sample stability. In this section, we discuss how **LoBoost** handles this.

At resolution level  $k$ , the partition cells are indexed by the prefix  $(L_1(x), \dots, L_k(x))$ , so the number of possible cells grows multiplicatively with the number of leaves of the first  $k$  trees. For gradient-boosted trees, this growth is governed primarily by the trees' `max_depth`: a depth- $d$  tree has at most  $2^d$  leaves, so in the worst case the number of cells can scale as  $O(2^{kd})$  when depths are roughly constant. Even if every tree is a decision stump ( $d = 1$ ), the number of cells is  $2^k$ . For this reason, we chose to dynamically increase the resolution level only for dense regions of the feature space.

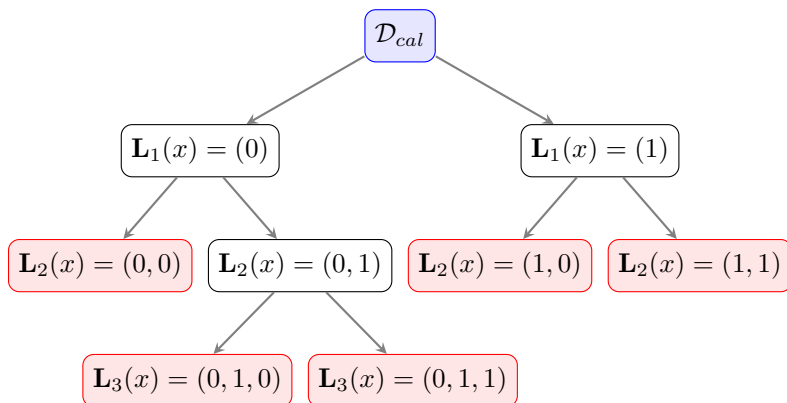


Figure 2: **LoBoost partition**. For convenience, we consider  $h_i(x)$  as decision stumps. White nodes indicate dense regions (at least  $N_{part}$  calibration instances) that proceed to the next resolution level. Red nodes denote terminal regions (less than  $N_{part}$  calibration instances). The example results in 5 terminal regions.

More precisely, given a set of calibration instances  $\mathcal{D}_{cal} = \{(X_i, Y_i)\}_{i=1}^m$ , we obtain their respective leaf identifiers  $\mathbf{L}_T(X_i)_{i=1}^m$ . At resolution level  $k$ , each region is formed by the

instances whose path coincide up until the  $k$ -th index. We increase the resolution level until all regions contain less than  $N_{part}$  instances, where  $N_{part}$  is a hyperparameter. In practice only regions with more than  $N_{part}$  instances proceed to a finer resolution level. Figure 2 illustrates this procedure.

Our partition algorithm is greedy: it keeps splitting dense regions until all are sparse. While this adaptivity prevents an explosion in the number of cells, it can also produce many regions that are too small for reliable local quantile estimation. We therefore follow the splitting stage with a region aggregation step.

To decide which sparse regions to merge, we use the similarity information already encoded by the boosting path. The leaf identifiers induce a multiscale notion of proximity: cells that share a long prefix  $(L_1, \dots, L_k)$  differ only in later trees, which typically make finer adjustments. As a result, disagreements in early coordinates tend to reflect meaningful differences in the predictor, whereas later discrepancies are often negligible. We operationalize this notion by defining a similarity measure on leaf identifiers: for two regions  $R$  and  $R'$ , define their weighted Hamming distance as

$$d_{\text{WH}}(R, R') = \sum_{t=1}^k w_t \mathbf{1}\{L_t(R) \neq L_t(R')\},$$

where the weights  $(w_t)_{t=1}^T$  are nonnegative and decreasing in  $t$ . A natural choice is an exponential decay  $w_t = \rho^t$  with  $\rho \in (0, 1)$ , which mirrors the geometric decay established in Corollary 1. More generally, the weights can be chosen in a data-driven manner by setting

$$w_t = \text{Var}[h_t(X)],$$

where the variance is estimated on the calibration set.

We iterate through regions of size smaller than  $N_{merge}$  (a hyperparameter), merging them into their respective most similar (minimum distance) region. We continue the process until all resulting regions have at a minimum  $N_{merge}$  instances. See Algorithm 1 for details.

Our implementation is open-source and available at [REDACTED](#)<sup>1</sup>. A key advantage of **LoBoost** is computational reuse: after fitting the boosting predictor, partition construction and calibration reuse its learned tree structure, with no retraining of the base model. Our implementation has native support for widely used Python boosting libraries, including scikit-learn’s gradient boosting (Pedregosa et al., 2011), XGBoost (Chen and Guestrin, 2016), and CatBoost (Prokhorenkova et al., 2019).

All the steps of our algorithm are computationally cheap:

- Leaf identifiers extraction is  $O(m \times T)$  at the worst case. We note that our algorithm dynamically increase the resolution level, typically yielding  $k \ll T$ , and consequently much reduced computation costs.
- Computing  $d_{\text{WH}}$  for a pair of regions requires  $O(k)$  operations. We compute all pairwise distances between regions, resulting in a total complexity of  $O(kp^2)$ , where  $p$  is the number of regions (partitions) before merging.

---

<sup>1</sup>The public repository link is temporarily redacted and will be released upon publication. For reproducibility, all code needed to run the experiments is included in the Supplementary Material.

## 5. Experiments

We compare the performance of our proposed approach against existing methods for constructing prediction regions. The methods compared in this section can be split in two groups: native methods, and model-based methods. This taxonomy is important because model-based methods require an additional training step, and therefore, a larger calibration set must be reserved.

**Native methods.** LoBoost and Inductive conformal prediction (ICP) (Vovk et al., 2005; Lei et al., 2018). ICP is the standard split/inductive conformal interval with absolute-residual scores and a single global calibration quantile. ICP is the most direct computational reference for LoBoost: both methods calibrate *post-hoc* on a fixed training/calibration split, require no retraining of the base regressor, and use the same fitted gradient-boosting model for point predictions. Thus, differences between ICP and LoBoost highlights reflect the benefit of local (partition-based) calibration.

Table 1: **Empirical marginal coverage** (AMC; closer to the nominal  $1 - \alpha = 90\%$  is better) on real-world datasets. All conformal methods are designed to achieve near-nominal coverage under exchangeability and do so consistently in our experiments, whereas the non-conformal NGBoost intervals can severely under-cover.

Dataset	Method					
	LoBoost	Locart	ICP	WICP	MICP	NGB
airfoil (1503, 5)	90.76 ( $\pm 0.83$ )	90.14 ( $\pm 0.69$ )	90.06 ( $\pm 0.57$ )	90.37 ( $\pm 0.51$ )	94.09 ( $\pm 0.43$ )	86.86 ( $\pm 0.57$ )
winered (1599, 11)	89.82 ( $\pm 0.65$ )	90.76 ( $\pm 0.62$ )	90.17 ( $\pm 0.55$ )	90.17 ( $\pm 0.56$ )	94.85 ( $\pm 0.44$ )	81.84 ( $\pm 0.71$ )
star (2161, 39)	89.44 ( $\pm 0.71$ )	89.79 ( $\pm 0.63$ )	89.72 ( $\pm 0.51$ )	89.59 ( $\pm 0.50$ )	91.71 ( $\pm 0.52$ )	82.04 ( $\pm 0.56$ )
winewhite (4898, 11)	89.96 ( $\pm 0.40$ )	90.08 ( $\pm 0.45$ )	90.12 ( $\pm 0.38$ )	89.97 ( $\pm 0.38$ )	90.67 ( $\pm 0.35$ )	87.29 ( $\pm 0.38$ )
cycle (9568, 4)	90.08 ( $\pm 0.29$ )	90.19 ( $\pm 0.31$ )	89.96 ( $\pm 0.25$ )	89.93 ( $\pm 0.20$ )	90.26 ( $\pm 0.22$ )	88.92 ( $\pm 0.24$ )
electric (10000, 12)	90.09 ( $\pm 0.34$ )	90.35 ( $\pm 0.30$ )	90.14 ( $\pm 0.24$ )	90.20 ( $\pm 0.25$ )	90.95 ( $\pm 0.23$ )	93.05 ( $\pm 0.19$ )
bike (10886, 18)	90.30 ( $\pm 0.27$ )	90.26 ( $\pm 0.20$ )	90.11 ( $\pm 0.22$ )	90.14 ( $\pm 0.21$ )	90.82 ( $\pm 0.24$ )	94.42 ( $\pm 0.16$ )
meps19 (15785, 139)	90.33 ( $\pm 0.23$ )	90.21 ( $\pm 0.20$ )	90.10 ( $\pm 0.16$ )	89.91 ( $\pm 0.19$ )	90.48 ( $\pm 0.19$ )	93.50 ( $\pm 0.13$ )
superconductivity (21263, 81)	90.41 ( $\pm 0.36$ )	90.46 ( $\pm 0.37$ )	89.95 ( $\pm 0.27$ )	90.08 ( $\pm 0.28$ )	90.57 ( $\pm 0.29$ )	91.73 ( $\pm 0.24$ )
WEC (54007, 98)	90.33 ( $\pm 0.26$ )	90.54 ( $\pm 0.40$ )	90.00 ( $\pm 0.27$ )	89.60 ( $\pm 0.35$ )	90.63 ( $\pm 0.24$ )	94.75 ( $\pm 0.13$ )
kernel (241600, 15)	90.13 ( $\pm 0.07$ )	90.25 ( $\pm 0.05$ )	89.95 ( $\pm 0.05$ )	90.00 ( $\pm 0.05$ )	90.02 ( $\pm 0.05$ )	93.14 ( $\pm 0.03$ )

Table 2: **Data-efficient UQ.** `LoBoost` is compared to the best-SMIS competing method on each dataset, reporting interval quality (SMIS), relative runtime (speedup), and the test MSE of the underlying point predictor. Because `LoBoost` does not require retraining or additional splits, it can allocate more data to training, yielding lower MSE for the fitted boosted model while keeping SMIS competitive with the best baseline. Values closer to 100% in the SMIS-efficiency column indicate interval quality closer to the best baseline; speedup values  $> 1$  indicate `LoBoost` is faster; and positive MSE-improvement values indicate lower test MSE than the best-SMIS baseline. Metric definitions are given in Appendix A.3.

Dataset	SMIS ( <code>LoBoost</code> )	Best SMIS	SMIS efficiency	Speedup	MSE improvement
airfoil (1503, 5)	13.83	11.73 (NGB)	84.79 %	2.48×	1.44 %
winered (1599, 11)	2.77	2.77 ( <code>LoBoost</code> )	100.00 %	1.00×	0.00 %
star (2161, 39)	960.27	956.59 (ICP)	99.62 %	0.10×	1.23 %
winewhite (4898, 11)	2.99	2.92 (MICP)	97.75 %	42.62×	2.37 %
cycle (9568, 4)	15.40	15.01 (MICP)	97.47 %	17.02×	3.62 %
electric (10000, 12)	0.05	0.05 (WICP)	96.46 %	19.43×	3.48 %
bike (10886, 18)	189.20	160.34 (WICP)	84.75 %	4.34×	6.09 %
meps19 (15785, 139)	72.73	67.46 (WICP)	92.75 %	25.02×	0.17 %
conductivity (21263, 81)	43.35	39.77 (WICP)	91.73 %	126.06×	5.39 %
WEC (54007, 98)	89040.88	69236.51 (MICP)	77.76 %	59.72×	4.55 %
kernel (241600, 15)	9.61	7.91 (WICP)	82.30 %	5.04×	5.22 %

**Model-based methods.** We also consider methods that obtain adaptivity by fitting additional nuisance components or by refitting the base learner on smaller effective training splits. *Weighted ICP (WICP)* (Lei et al., 2018) uses weighted nonconformity scores to adapt interval widths under heteroscedasticity, requiring an auxiliary model (e.g., a scale/MAD estimator) trained on held-out data. *Mondrian ICP (MICP)* (Boström and Johansson, 2020) performs conformal calibration within difficulty-based bins, where the difficulty score is estimated from data and calibration is carried out separately per bin. *LoCART* (Cabezas et al., 2025b) is a partition-based conformal method that learns tree-induced local groups (via an auxiliary tree/partitioning step) to target local validity. Finally, *NGBoost (NGB)* (Duan et al., 2020) is a non-conformal probabilistic boosting approach that constructs prediction intervals from an estimated conditional distribution; unlike conformal methods, it does not guarantee finite-sample coverage. Implementation details and hyperparameter choices for all benchmarks are provided in the Supplementary Material A.2.

In all experiments, we split the dataset into training, calibration, and test sets with proportions of 0.4, 0.4, and 0.2, respectively. For native methods, we incorporated 30% of the calibration set into the training set.

We evaluate prediction regions using: **marginal coverage** (how often the interval contains the true test response), **SMIS** (an interval scoring rule that rewards shorter intervals but penalizes misses outside the bounds, capturing both sharpness and reliability), **test MSE** (point-prediction accuracy of the underlying regressor), and **calibration time** (wall-clock cost of the post-hoc conformal calibration step). Full metric details are provided in the Supplementary Material (Appendix A.3).

Dataset descriptions and complete results are provided in Supplementary Material C. We include problems spanning a wide range of sample sizes and feature dimensions to benchmark `LoBoost` against multiple baselines.

## 5.1. Results

**Coverage and reliability.** Table 1 shows that the conformal baselines achieve near-nominal marginal coverage across datasets, as expected. In contrast, NGBoost can *severely under-cover* in several settings, with empirical coverage falling well below the  $1 - \alpha = 0.9$  target (especially on smaller datasets), highlighting the fragility of distributional assumptions in finite samples.

**Data efficiency and post-hoc calibration cost.** Table 2 summarizes the main practical advantage of LoBoost. Because LoBoost is *post-hoc* and does not require retraining or additional data splits, we can allocate more data to fitting the underlying point predictor. This yields a consistent reduction in test MSE relative to the best-SMIS baseline, while keeping SMIS close to the strongest competing method. At the same time, LoBoost provides substantial calibration-time savings: the speedup vs the best-SMIS baseline is often one to two orders of magnitude on medium/large datasets. Overall, LoBoost delivers a favorable speed-accuracy-uncertainty trade-off by improving the base predictor and maintaining competitive interval quality.

**ICP-level runtime with improved interval quality.** To isolate the effect of locality (independent of retraining-based baselines), Table 3 compares LoBoost directly to standard ICP. LoBoost retains essentially the same calibration-time profile as ICP, but achieves noticeably better SMIS on the majority of datasets, indicating improved local adaptivity (i.e., better calibrated intervals across heterogeneous regions) at ICP-like computational cost.

Table 3: **LoBoost vs ICP.** LoBoost matches the computational profile of standard inductive conformal prediction (ICP) while achieving consistently better interval quality (SMIS), indicating improved local adaptivity/coverage behavior at essentially the same runtime.

Dataset	SMIS (LoBoost)	SMIS (ICP)	SMIS efficiency
airfoil (1503, 5)	13.83	15.40	111.31 %
winered (1599, 11)	2.77	2.79	100.93 %
star (2161, 39)	960.27	956.59	99.62 %
winewhite (4898, 11)	2.99	3.03	101.36 %
cycle (9568, 4)	15.40	15.59	101.21 %
electric (10000, 12)	0.05	0.06	103.34 %
bike (10886, 18)	189.20	217.32	114.86 %
meps19 (15785, 139)	72.73	96.13	132.17 %
conductivity (21263, 81)	43.35	53.29	122.93 %
WEC (54007, 98)	89040.88	111665.36	125.41 %
kernel (241600, 15)	9.61	13.61	141.59 %

## 6. Final remarks

LoBoost provides a simple, model-native route to local conformal prediction for gradient-boosted trees by reusing the partition already induced by the trained ensemble, rather than

learning an auxiliary partition or nuisance model. This design preserves data efficiency—no retraining and no additional splitting beyond the standard train/calibration split—and translates into strong empirical performance: interval quality remains competitive with the strongest local baselines (SMIS efficiency 77.8%–99.6%), while point accuracy improves on 10/11 datasets (typically by 3–4%, and up to about 5–6% in test MSE). At the same time, calibration is substantially faster (median 17× and up to 126× speedup). From an implementation standpoint, `LoBoost` only requires access to leaf indices along the boosting path, making it straightforward to integrate with standard libraries such as `XGBoost`, `LightGBM`, and `CatBoost`. Our theory links boosting stability to within-cell residual homogeneity, yielding asymptotic conditional validity while preserving finite-sample marginal coverage.

## Acknowledgements

Rafael Izbicki is grateful for the financial support of CNPq (422705/2021-7, 305065/2023-8 and 403458/2025-0) and FAPESP (grant 2023/07068-1). Luben M. C. Cabezas is grateful for the financial support of FAPESP (grants 2022/08579-7 and 2025/06168-8). Thiago R. Ramos is grateful for the financial support of CNPq (403458/2025-0). Vagner S. Santos is grateful for the financial support of FAPESP (grant 2023/05587-1).

## References

- Angelopoulos, A. N., Bates, S., et al. (2023). Conformal prediction: A gentle introduction. *Foundations and trends® in machine learning*, 16(4):494–591.
- Boström, H. and Johansson, U. (2020). Mondrian conformal regressors. In *Conformal and probabilistic prediction and applications*, pages 114–133. PMLR.
- Cabezas, L., Santos, V. S., Ramos, T. R., Rodrigues, P. L., and Izbicki, R. (2025a). Cp4sbi: Local conformal calibration of credible sets in simulation-based inference. *arXiv preprint arXiv:2508.17077*.
- Cabezas, L. M., Otto, M. P., Izbicki, R., and Stern, R. B. (2025b). Regression trees for fast and adaptive prediction intervals. *Information Sciences*, 686:121369.
- Cabezas, L. M. C., Santos, V. S., Ramos, T., and Izbicki, R. (2025c). Epistemic uncertainty in conformal scores: A unified approach. In *The 41st Conference on Uncertainty in Artificial Intelligence*.
- Cabezas, L. M. C., Soares, G. P., Ramos, T. R., Stern, R. B., and Izbicki, R. (2025d). Conformal calibration of statistical confidence sets.
- Chen, T. and Guestrin, C. (2016). Xgboost: A scalable tree boosting system. In *Proceedings of the 22nd acm sigkdd international conference on knowledge discovery and data mining*, pages 785–794.
- Chernozhukov, V., Wüthrich, K., and Zhu, Y. (2021). Distributional conformal prediction. *Proceedings of the National Academy of Sciences*, 118(48):e2107794118.

- Dheur, V., Bosser, T., Izbicki, R., and Ben Taieb, S. (2024). Distribution-free conformal joint prediction regions for neural marked temporal point processes. *Machine Learning*, 113(9):7055–7102.
- Duan, T., Anand, A., Ding, D. Y., Thai, K. K., Basu, S., Ng, A., and Schuler, A. (2020). Ngboost: Natural gradient boosting for probabilistic prediction. In *International conference on machine learning*, pages 2690–2700. PMLR.
- Fang, H., Tan, K., and Hooker, G. (2025). Statistical inference for gradient boosting regression. In *The Thirty-ninth Annual Conference on Neural Information Processing Systems*.
- Foygel Barber, R., Candes, E. J., Ramdas, A., and Tibshirani, R. J. (2021). The limits of distribution-free conditional predictive inference. *Information and Inference: A Journal of the IMA*, 10(2):455–482.
- Friedman, J. H. (2001). Greedy function approximation: a gradient boosting machine. *Annals of statistics*, pages 1189–1232.
- Fröhlich, A., Ramos, T., Dos Santos, G. M. C., Buzatto, I. P. C., Izbicki, R., and Tiezzi, D. G. (2025). Personalizedus: Interpretable breast cancer risk assessment with local coverage uncertainty quantification. In *Proceedings of the AAAI Conference on Artificial Intelligence*, volume 39, pages 27998–28006.
- Gneiting, T. and Raftery, A. (2007). Strictly proper scoring rules, prediction, and estimation. *Journal of the American Statistical Association*, 102(477):359–378.
- Grinsztajn, L., Oyallon, E., and Varoquaux, G. (2022). Why do tree-based models still outperform deep learning on typical tabular data? *Advances in neural information processing systems*, 35:507–520.
- Grubb, A. and Bagnell, J. A. (2012). Generalized boosting algorithms for convex optimization.
- Guan, L. (2023). Localized conformal prediction: A generalized inference framework for conformal prediction. *Biometrika*, 110(1):33–50.
- Izbicki, R. (2025). *Machine Learning Beyond Point Predictions: Uncertainty Quantification*. 1st edition.
- Izbicki, R., Shimizu, G., and Stern, R. (2020). Flexible distribution-free conditional predictive bands using density estimators. In *International Conference on Artificial Intelligence and Statistics*, pages 3068–3077. PMLR.
- Izbicki, R., Shimizu, G., and Stern, R. B. (2022). Cd-split and hpd-split: Efficient conformal regions in high dimensions. *Journal of Machine Learning Research*, 23(87):1–32.
- Jung, C., Noarov, G., Ramalingam, R., and Roth, A. (2023). Batch multivalid conformal prediction. In *International Conference on Learning Representations (ICLR)*.

- Kiyani, S., Pappas, G. J., and Hassani, H. (2024). Conformal prediction with learned features. In *International Conference on Machine Learning*, pages 24749–24769. PMLR.
- Lai, Y., Zheng, P., Ji, C., Qiu, C., Wang, T., Zhang, S., Wang, Z., and Du, Y. (2025). Coffeeboost: Gradient boosting native conformal inference for bayesian optimization. In *Proceedings of the AAAI Conference on Artificial Intelligence*, volume 39, pages 18017–18025.
- Lei, J., G’Sell, M., Rinaldo, A., Tibshirani, R. J., and Wasserman, L. (2018). Distribution-free predictive inference for regression. *Journal of the American Statistical Association*, 113(523):1094–1111.
- Lei, J. and Wasserman, L. (2014). Distribution-free prediction bands for non-parametric regression. *Journal of the Royal Statistical Society Series B: Statistical Methodology*, 76(1):71–96.
- Linusson, H., Norinder, U., Boström, H., Johansson, U., and Löfström, T. (2017). On the calibration of aggregated conformal predictors. In *Conformal and probabilistic prediction and applications*, pages 154–173. PMLR.
- Martinez, N., Patel, D. C., Reddy, C., Ganapavarapu, G., Vaculin, R., and Kalagnanam, J. (2024). Identifying homogeneous and interpretable groups for conformal prediction. In *The 40th Conference on Uncertainty in Artificial Intelligence*.
- Pedregosa, F., Varoquaux, G., Gramfort, A., Michel, V., Thirion, B., Grisel, O., Blondel, M., Prettenhofer, P., Weiss, R., Dubourg, V., Vanderplas, J., Passos, A., Cournapeau, D., Brucher, M., Perrot, M., and Duchesnay, E. (2011). Scikit-learn: Machine learning in Python. *Journal of Machine Learning Research*, 12:2825–2830.
- Prokhorenkova, L., Gusev, G., Vorobev, A., Dorogush, A. V., and Gulin, A. (2019). Catboost: unbiased boosting with categorical features.
- Ramos, T., Loro Schuller, R., Akira Okuno, A., Nissenbaum, L., I Oliveira, R., and Orenstein, P. (2024). Blockboost: Scalable and efficient blocking through boosting. In Dasgupta, S., Mandt, S., and Li, Y., editors, *Proceedings of The 27th International Conference on Artificial Intelligence and Statistics*, volume 238 of *Proceedings of Machine Learning Research*, pages 2575–2583. PMLR.
- Romano, Y., Patterson, E., and Candes, E. (2019). Conformalized quantile regression. *Advances in neural information processing systems*, 32.
- Shafer, G. and Vovk, V. (2008). A tutorial on conformal prediction. *Journal of Machine Learning Research*, 9(3).
- Shakhnarovich, G. (2005). *Learning Task-Specific Similarity*. PhD thesis, Massachusetts Institute of Technology. Ph.D. thesis.
- Sprangers, O., Schelter, S., and de Rijke, M. (2021). Probabilistic gradient boosting machines for large-scale probabilistic regression. In *Proceedings of the 27th ACM SIGKDD conference on knowledge discovery & data mining*, pages 1510–1520.

- van der Vaart, A. W. (1998). *Asymptotic Statistics*. Cambridge University Press.
- Vovk, V. (2012). Conditional validity of inductive conformal predictors. In *Asian conference on machine learning*, pages 475–490. PMLR.
- Vovk, V., Gammerman, A., and Shafer, G. (2005). *Algorithmic learning in a random world*, volume 29. Springer.
- Xie, R., Barber, R., and Candes, E. (2024). Boosted conformal prediction intervals. *Advances in Neural Information Processing Systems*, 37:71868–71899.
- Xu, Y., Liaw, A., Sheridan, R. P., and Svetnik, V. (2024). Development and evaluation of conformal prediction methods for quantitative structure–activity relationship. *ACS omega*, 9(27):29478–29490.
- Zhou, X., Chen, B., Gui, Y., and Cheng, L. (2025). Conformal prediction: A data perspective. *ACM Computing Surveys*.

# LoBoost : Local Conformal Prediction with Boosting-Induced Partitions (Supplementary Material)

Vagner Silva Santos<sup>1,2</sup>, Victor Coscrato<sup>1</sup>, Luben M. C. Cabezas<sup>1,2,3</sup>,  
Rafael Izbicki<sup>1</sup>, and Thiago R. Ramos<sup>1</sup>

<sup>1</sup> Department of Statistics, Federal University of São Carlos, São Carlos, São Paulo, Brazil

<sup>2</sup> Institute of Mathematics and Computer Science, University of São Paulo, São Carlos, São  
Paulo, Brazil

<sup>3</sup> Université Grenoble Alpes, Inria, CNRS, Grenoble INP, LJK, France

February 27, 2026

## A. Experiments Evaluation

### A.1. Gradient boosting base model and hyperparameters

Across all methods and datasets, we use the same Gradient Boosting regressor to estimate the point prediction function  $\hat{\mu}(\cdot)$ . We tune hyperparameters via `GridSearchCV` with 5-fold cross-validation on the training split, using the following grid:

- `max_depth`  $\in \{3, 4, 5\}$ ,
- `min_samples_leaf`  $\in \{100, 200\}$ ,
- `subsample` = 0.8,
- `learning_rate`  $\in \{0.1, 0.05\}$ .

After selecting the best configuration, we train the final model with:

- `n_estimators`= 1000,
- `validation_fraction`= 0.1,
- `n_iter_no_change`= 15 (early stopping).

### A.2. Benchmark Models

We evaluate the performance of our proposed method against the following baselines:

- **Inductive conformal prediction (ICP)** (Vovk et al. (2005); Lei et al. (2018)): implemented in the *nonconformist* library Linusson et al. (2017). This baseline represents the standard inductive conformal prediction intervals approach, where the miscoverage level is the sole hyperparameter.
- **Weighted ICP (WICP)** (Lei et al., 2018): Implemented in the *clover* library, which is detailed in Cabezas et al. (2025b). We employ a Random Forest regressor to estimate the mean absolute deviation of the residuals, allowing for heteroscedastic interval widths. The only hyperparameter is the miscoverage level.
- **Mondrian-split (MICP)** (Boström and Johansson, 2020): Implemented in the *clover* library, which is detailed in Cabezas et al. (2025b). We utilize the default difficulty estimator (the variance of predictions across the Random Forest trees). Difficulty estimates were partitioned into  $k = 30$  bins based on the quantiles  $(1/k, 2/k, \dots, \frac{k-1}{k}, 1)$ .
- **LoCART** (Cabezas et al. (2025b)): A nonconformity method based on partitioning the feature space by training a Decision Tree regression model to learn the non-conformity score. This approach guarantees a asymptotic local coverage. Detailed implementation details are available in the *clover*.
- **Natural Gradient Boosting (NGB)** (Duan et al., 2020) : Use as a probabilistic boosting baseline. Unlike conformal methods, NGB estimates the parameters of a conditional probability distribution, typically yielding prediction intervals based on the estimated quantiles of a normal distribution.

For the conformal baselines, the significance level was set to  $\alpha$ . In *LoBoost*, we used  $M = 200$  with the weighted Hamming merge method. *LoCART* was configured with `min_samples_leaf = 150`, `criterion = squared_error`, tree pruning enabled, no random projections,  $m = 300$ , and  $h = 20$ . Mondrian ICP used  $k = 30$  bins. Normalized Gradient Boosting (NGB) was evaluated with `early_stopping_rounds = 30`. All other parameters were kept at their default values as defined in the experimental framework and in their respective libraries.

### A.3. Evaluation Metrics

#### A.3.1. Absolute Metrics

We formally define the evaluation metrics used to assess the quality of the prediction regions. These metrics quantify both *validity*, through coverage properties, and *efficiency*, through measures of interval length and scoring rules. All metrics are computed on the test set  $I_{\text{test}}$ , and, when applicable, are reported relative to the nominal coverage level  $1 - \alpha$ . We conducted 50 independent data splits to estimate the mean performance metrics and their associated standard errors, considering a 5% significance level.

- **Average Marginal Coverage (AMC)**: This metric measures the proportion of test points whose true outcome  $Y_i$  falls within the prediction region  $\hat{C}(X_i)$ . In summary,

we estimate  $\mathbb{P}[Y \in C(\mathbf{X}_i)]$  using

$$AMC = \frac{1}{|I_{\text{test}}|} \sum_{(\mathbf{X}_i, y_i) \in I_{\text{test}}} \mathbb{I}(y_i \in C(\mathbf{X}_i))$$

where  $\mathbb{I}(\cdot)$  is the indicator function. For a valid prediction interval, this value should be close to the nominal coverage level,  $1 - \alpha$ .

- **Average Interval Length (IL):** This measures the average size or width of the prediction regions,

$$IL = \frac{1}{|I_{\text{test}}|} \sum_{\mathbf{X}_i \in I_{\text{test}}} |\hat{C}(X_i)|,$$

where  $|\hat{C}(X_i)| = |\max \hat{C}(X_i) - \min \hat{C}(X_i)|$  denotes the length of the region. A smaller interval length indicates a more efficient and informative prediction, provided that the marginal coverage requirement is met.

- **Standard Mean Interval Score (SMIS):** The SMIS, from Gneiting and Raftery (2007), is utilized to assess the conditional coverage validity of predictive intervals, particularly when evaluated on real-world data where the true data distribution is unknown. The Interval Score (IS) penalizes the true observation  $y$  based on its position relative to the prediction interval, factoring in the miscoverage level  $\alpha$  and the interval length, as defined by the following equation:

$$\begin{aligned} \text{IS}_\alpha(\hat{C}(\mathbf{X}_i), y) = & \left[ \left( \max \hat{C}(\mathbf{X}_i) - \min \hat{C}(\mathbf{X}_i) \right) \right. \\ & + \frac{2}{\alpha} \left( \min \hat{C}(\mathbf{X}_i) - y \right) \mathbb{I}(y < \min \hat{C}(\mathbf{X}_i)) \\ & \left. + \frac{2}{\alpha} \left( y - \max \hat{C}(\mathbf{X}_i) \right) \mathbb{I}(y > \max \hat{C}(\mathbf{X}_i)) \right] \end{aligned}$$

where  $\min \hat{C}(\mathbf{X}_i)$  and  $\max \hat{C}(\mathbf{X}_i)$  are the minimum and maximum of the (closed) prediction interval  $\hat{C}(\mathbf{X})$ . Thus, the SMIS is defined as the average of the Interval Scores ( $\text{IS}_\alpha$ ) across the test set  $I_{\text{test}}$ , as shown below:

$$\text{SMIS}_\alpha = \frac{1}{|I_{\text{test}}|} \sum_{(\mathbf{X}_i, y_i) \in I_{\text{test}}} \text{IS}_\alpha(\hat{C}(\mathbf{X}_i), y_i).$$

By construction, lower values indicate better forecasts.

### A.3.2. Relative Metrics

We also report relative metrics that compare `LoBoost` to the strongest baseline on each dataset. Let `best` denote the competing baseline method with the best (highest) SMIS among those considered.

- **SMIS efficiency.** This metric measures how close the interval quality of `LoBoost`

is to the best baseline, in percentage terms:

$$\text{SMIS-efficiency} = 100 \cdot \frac{\text{SMIS}(\text{best})}{\text{SMIS}(\text{LoBoost})}.$$

Values closer to 100% indicate that `LoBoost` matches the interval quality of the best baseline; values above (below) 100% indicate that `LoBoost` is worse (better) in terms of SMIS.

- **Speedup.** This metric compares post-hoc calibration time (or prediction-set construction time) between methods:

$$\text{Speedup} = \frac{\text{Time}(\text{best})}{\text{Time}(\text{LoBoost})}.$$

Values  $> 1$  mean `LoBoost` is faster than the best-SMIS baseline (higher is better), while values  $< 1$  mean it is slower.

- **MSE improvement (relative point-prediction error).** This metric compares the test MSE of the underlying point predictor used by each method:

$$\text{MSE-improvement} = 100 \cdot \left( \frac{\text{MSE}(\text{best})}{\text{MSE}(\text{LoBoost})} - 1 \right).$$

Positive values indicate that `LoBoost` achieves lower test MSE than the best-SMIS baseline.

#### A.4. Simulation Experiments

- Our simulation study described in Fig. 1 is based on the conditional distribution of the response variable  $Y$  given the feature  $X$ . The feature  $X$  is drawn from a uniform distribution,  $X \sim \text{U}[-2, 2]$ . The response variable  $Y$  is conditionally distributed as a Gaussian:

$$Y \mid X = x \sim \mathcal{N}(\mu(x), \sigma^2(x)),$$

where the mean function is defined as  $\mu(x) = 3 \sin(x)$ . The conditional standard deviation  $\sigma(x)$  follows a piecewise constant structure (with a sample-dependent term for the final partition), defined as follows:

$$\sigma(x) = \begin{cases} 0.8 & \text{if } x < -0.8 \\ 2.0 & \text{if } -0.8 \leq x < 0.1 \\ 1 & \text{if } 0.1 \leq x < 1.4 \\ x^2 & \text{if } x \geq 1.4 \end{cases}$$

This scenario is specifically designed to evaluate the performance of our proposed approach in settings characterized by abrupt heteroscedasticity. By introducing a significantly higher noise level ( $\sigma = 2.0$ ) in the second interval and a non-linear variance component in the fourth, this setup tests the model’s ability to produce locally adaptive predictive intervals. Such characteristics are essential for capturing aleatoric uncertainty that varies sharply across different regions of the feature space.

- In the second scenario, we evaluate a setting where the feature space exhibits a structural gap, resulting in discontinuous support for the covariate distribution. Specifically, we define the feature space as  $\mathcal{X} = [-2, -0.5) \cup (0.8, 2]$ , thereby inducing a region with null support in the interval  $[-0.5, 0.8]$ .

The conditional distribution of the response remains Gaussian,

$$Y | X = x \sim \mathcal{N}(\mu(x), \sigma^2(x)),$$

but both the mean and variance functions depend on the regime. Specifically, the data generating process is defined as:

$$\mu(x) = \begin{cases} -2x - 1 & \text{if } x < -0.5, \\ 2 \sin(3x) & \text{if } x > 0.8, \end{cases}$$

$$\sigma(x) = \begin{cases} 0.3 & \text{if } x < -0.5, \\ 0.2 + 0.5x^2 & \text{if } x > 0.8. \end{cases}$$

This configuration introduces two distinct data-generating regimes separated by a region without covariate support. The absence of observations in the central interval induces extrapolation, making this scenario particularly suitable for assessing how predictive intervals behave under support mismatch and structural regime shifts. This setting is especially challenging for globally smooth models, which may incorrectly interpolate across the unsupported region.

As in both settings, we simulate from a Gaussian distribution and directly compute the oracle prediction region (Oracle Interval) for new points, defined as:

$$OI(Y, 1 - \alpha) = [\mu(x) - z_{\alpha/2}\sigma(x), \mu(x) + z_{\alpha/2}\sigma(x)],$$

where  $z_{\alpha/2}$  is the  $\alpha/2$  quantile of the standard Gaussian distribution. The Oracle Interval is useful for assessing how close a given method is to the true prediction interval.

## B. Algorithm Details

We recall the weighted Hamming distance used throughout the aggregation step to quantify similarity between boosting-induced regions:

$$d_{\text{WH}}(R, R') = \sum_{t=1}^k w_t \mathbf{1}\{L_t(R) \neq L_t(R')\}, \quad (2)$$

---

### Algorithm 1 Tree-Based Partitioning and Aggregation

---

**Require:** Calibration data  $\mathcal{D}_{\text{cal}}$ , non-conformity score function  $s(x, y)$ , significance level  $\alpha$ , minimum samples  $M$ , pre-trained Boosting model of  $T$  trees.

**Ensure:** Partition dictionary  $\mathcal{P}$  with computed quantiles  $\hat{q}$ .

- 1: Extract leaf indices  $L \in \mathbb{R}^{m \times T}$  for all  $X_i$  through the ensemble.
  - 2: Let  $\mathcal{T}$  be an empty partition tree.
  - 3: Initialize  $\mathcal{G} = \{(\mathcal{D}, \mathcal{T}, \emptyset)\}$  ▷ Active groups: (data, node, path)
  - 4: **for** each tree  $t \in \{1, \dots, T\}$  **do**
  - 5:      $\mathcal{G}_{\text{next}} \leftarrow \emptyset$
  - 6:     **for** each  $(D_g, \text{node}, \text{path}) \in \mathcal{G}$  **do** ▷  $D_g = \{x : L_j(x) = L_j(x') \text{ for all } j < t\}$ .
  - 7:         **if**  $|D_g| < M$  **then**
  - 8:             Mark node as *terminal* and assign partition ID.
  - 9:             **else if** all samples in  $D_g$  fall into the same leaf in tree  $t$  **then**
  - 10:                 Create *ignore* (tunneling) branch in  $\mathcal{T}$ .
  - 11:                 Add to  $\mathcal{G}_{\text{next}}$  with path  $\text{path} \cup \{\text{ignore}\}$ .
  - 12:             **else**
  - 13:                 Split  $D_g$  into children  $\{D_{g,l}\}$  based on unique leaves  $l$  at tree  $t$ .
  - 14:                 Add each  $(D_{g,l}, \text{node}_l, \text{path} \cup \{l\})$  to  $\mathcal{G}_{\text{next}}$ .
  - 15:             **end if**
  - 16:     **end for**
  - 17:      $\mathcal{G} \leftarrow \mathcal{G}_{\text{next}}$
  - 18: **end for**
  - 19: Compute tree weights  $w_t$  based on feature importance or predictive performance.
  - 20: Let  $S$  be the set of partitions where  $|D_g| < M$  and  $L$  where  $|D_g| \geq M$ .
  - 21: **for** each  $R \in S$  **do**
  - 22:      $R^* \leftarrow \arg \min_{R' \in L} d_{\text{WH}}(R, R')$  ▷ Merge using weighted path similarity by (2)
  - 23:     Merge  $R$  into  $R^*$
  - 24: **end for**
  - 25:  $\mathcal{P} \leftarrow$  Final aggregated regions.
  - 26: **for** each partition  $P \in \mathcal{P}$  **do**
  - 27:      $\hat{q}_P \leftarrow \text{Quantile}(\{s(X_i, Y_i) : (X_i, Y_i) \in P\}, 1 - \alpha)$
  - 28: **end for**
  - 29: **return**  $\{P : (D_P, \hat{q}_P)\}$
-

## C. Supplementary Results for Real-World Datasets

This section presents additional experimental results on real-world datasets used to evaluate the proposed method. We provide a detailed description of each dataset, including the number of instances and features (see Table 4, followed by comprehensive performance tables reporting all evaluation metrics, as well as additional analyses that provide further insight into the behavior of `LoBoost` .

Table 4: Summary of Real-World Datasets

Dataset	Instances (n)	Features (p)
airfoil	1,503	5
bike	10,886	18
superconductivity	21,263	81
cycle	9,568	4
electric	10,000	12
kernel	241,600	15
meps19	15,785	139
star	2,161	39
Wave Energy Converter (WEC)	54,007	98
winewhite	4,898	11
winered	1,599	11

To handle scenarios in which the feature space requires partitioning and the dependence of  $Y$  on  $X$  is heteroscedastic, it is necessary to analyze the number of partitions generated by LoBoost and compare it with LoCART, another method from the literature that explicitly constructs partitions in the feature space. Table 5 shows that LoBoost tends to detect more partitions in the feature space compared to LoCART. Moreover, in order to guarantee well-calibrated splits, the merging mechanism appears to be functioning effectively.

Table 5: **LoBoost Partition Dynamics.** The results are obtained over the specified iterations, with standard errors reported at the 95% confidence level.

<b>Dataset</b>	LoBoost-Pre	LoBoost-Final	LoBoost-Merge	LoCART
airfoil	5.80 ( $\pm 0.43$ )	1.66 ( $\pm 0.17$ )	4.14 ( $\pm 0.34$ )	1.00 ( $\pm 0.00$ )
winered	6.26 ( $\pm 0.41$ )	1.56 ( $\pm 0.20$ )	4.70 ( $\pm 0.25$ )	1.00 ( $\pm 0.00$ )
star	9.26 ( $\pm 0.60$ )	2.18 ( $\pm 0.21$ )	7.08 ( $\pm 0.49$ )	2.00 ( $\pm 0.00$ )
winewhite	22.64 ( $\pm 1.23$ )	3.56 ( $\pm 0.33$ )	19.08 ( $\pm 1.05$ )	2.66 ( $\pm 0.40$ )
bike	57.68 ( $\pm 1.52$ )	11.66 ( $\pm 0.36$ )	46.02 ( $\pm 1.47$ )	7.64 ( $\pm 0.69$ )
cycle	45.02 ( $\pm 1.28$ )	8.22 ( $\pm 0.55$ )	36.80 ( $\pm 1.08$ )	3.80 ( $\pm 0.77$ )
electric	78.94 ( $\pm 3.63$ )	9.50 ( $\pm 0.43$ )	69.44 ( $\pm 3.32$ )	4.84 ( $\pm 0.79$ )
meps19	106.50 ( $\pm 3.95$ )	22.00 ( $\pm 0.51$ )	84.50 ( $\pm 3.95$ )	8.56 ( $\pm 1.07$ )
superconductivity	173.07 ( $\pm 9.07$ )	27.07 ( $\pm 1.12$ )	146.00 ( $\pm 9.15$ )	11.47 ( $\pm 3.59$ )
kernel	1034.16 ( $\pm 8.92$ )	327.56 ( $\pm 1.30$ )	706.60 ( $\pm 8.84$ )	160.16 ( $\pm 8.28$ )
WEC	384.60 ( $\pm 12.01$ )	75.00 ( $\pm 1.57$ )	309.60 ( $\pm 12.70$ )	38.73 ( $\pm 4.55$ )

Table 6: **Average Interval Length results.** The results are obtained over the specified iterations, with standard errors reported at the 95% confidence level.

Dataset	Type of method					
	Conformal					Non-conformal
	LoBoost	Locart	ICP	WICP	MICP	NGB
airfoil (1503, 5)	10.4749 (±0.2666)	11.5611 (±0.2728)	11.4770 (±0.1988)	10.9139 (±0.1646)	15.1056 (±0.2451)	<b>8.4415</b> (± <b>0.0765</b> )
bike (10886, 18)	128.6475 (±1.7026)	128.7410 (±1.7817)	137.1908 (±1.7248)	<b>123.2579</b> (± <b>1.3208</b> )	131.3161 (±1.5278)	223.7452 (±1.0477)
cycle (9568, 4)	11.2960 (±0.1111)	11.5021 (±0.1014)	11.4035 (±0.0767)	<b>11.0605</b> (± <b>0.0612</b> )	11.1988 (±0.0624)	11.5290 (±0.0386)
electric (10000, 12)	0.0419 (±0.0004)	0.0430 (±0.0003)	0.0427 (±0.0002)	<b>0.0411</b> (± <b>0.0002</b> )	0.0443 (±0.0003)	0.0485 (±0.0003)
kernel (241600, 15)	5.8746 (±0.0341)	5.4835 (±0.0364)	5.5315 (±0.0277)	<b>5.2142</b> (± <b>0.0237</b> )	5.6061 (±0.0324)	6.6800 (±0.0152)
meps19 (15785, 139)	31.5907 (±0.9537)	30.4999 (±0.8556)	33.7961 (±0.4807)	<b>23.6475</b> (± <b>0.7356</b> )	31.6198 (±0.5509)	31.8853 (±0.3965)
star (2161, 39)	775.5698 (±10.7328)	781.1618 (±9.2175)	780.3686 (±4.7723)	780.8040 (±5.3272)	855.6615 (±7.2150)	<b>645.4459</b> (± <b>3.5887</b> )
superconductivity (21263, 81)	29.8581 (±0.6004)	29.9623 (±0.7434)	32.9386 (±0.5608)	<b>25.8190</b> (± <b>0.3725</b> )	27.5716 (±0.4829)	36.1783 (±0.2186)
WEC (54007, 98)	49512.9772 (±975.4950)	48626.3277 (±986.8975)	52169.3237 (±1109.2854)	<b>35780.4857</b> (± <b>1382.0722</b> )	44956.9192 (±1193.3323)	123877.8887 (±972.2280)
winered (1599, 11)	2.0556 (±0.0372)	2.1243 (±0.0359)	2.0787 (±0.0244)	2.1227 (±0.0357)	2.7408 (±0.0404)	<b>1.5206</b> (± <b>0.0132</b> )
winewhite (4898, 11)	2.2527 (±0.0240)	2.2828 (±0.0236)	2.2809 (±0.0198)	2.2641 (±0.0190)	2.3147 (±0.0203)	<b>2.0429</b> (± <b>0.0073</b> )

In Table 6, we generally observe the strong performance of WICP in constructing prediction intervals with smaller average lengths, while LoBoost achieves comparably competitive values. In particular, for datasets with a small number of observations, NGB produces the shortest prediction intervals. However, this comes at the cost of undercoverage in these datasets (see Table 1).

In contrast, all conformal methods maintain coverage levels close to the nominal marginal level. Notably, LoBoost achieves a favorable balance by combining relatively low average interval length with coverage that remains close to the nominal level.

Analyzing the SMIS results in Table 7 across all methods, we observe that, overall, WICP — a method based on retraining and weight assignment — achieves the best performance. In particular, WICP tends to construct compact prediction intervals while maintaining a low interval error rate.

However, LoBoost remains competitive with WICP in terms of SMIS. Moreover, it is important to consider the substantially lower calibration time of LoBoost (see Table 8) compared to the best-performing method in terms of SMIS, as well as when combined with a more powerful predictive model (see Table 9).

Table 7: **SMIS Results.** The results are obtained over the specified iterations, with standard errors reported at the 95% confidence level.

Dataset	Type of method					
	LoBoost	Locart	ICP	WICP	MICP	NGB
airfoil (1503, 5)	13.8344 (±0.3053)	15.4463 (±0.3418)	15.3985 (±0.3426)	13.4449 (±0.2390)	17.3529 (±0.2863)	<b>11.7296</b> (±0.2411)
winered (1599, 11)	<b>2.7668</b> (±0.0442)	<b>2.7997</b> (±0.0421)	<b>2.7925</b> (±0.0436)	<b>2.8046</b> (±0.0435)	3.0725 (±0.0394)	2.9622 (±0.0714)
star (2161, 39)	<b>960.2747</b> (±10.5618)	<b>961.1148</b> (±9.7679)	<b>956.5903</b> (±9.7525)	<b>960.6974</b> (±9.9493)	1001.1475 (±9.6525)	1013.9909 (±14.3376)
winewhite (4898, 11)	2.9916 (±0.0303)	3.0229 (±0.0319)	3.0322 (±0.0320)	<b>2.9733</b> (±0.0313)	<b>2.9243</b> (±0.0276)	2.9864 (±0.0337)
cycle (9568, 4)	15.3992 (±0.1789)	15.5445 (±0.1548)	15.5862 (±0.1572)	<b>15.0424</b> (±0.1537)	<b>15.0089</b> (±0.1576)	15.9588 (±0.1548)
electric (10000, 12)	0.0546 (±0.0004)	0.0557 (±0.0004)	0.0564 (±0.0004)	<b>0.0527</b> (±0.0003)	0.0552 (±0.0003)	0.0570 (±0.0004)
bike (10886, 18)	189.1999 (±2.3041)	187.7402 (±2.4479)	217.3228 (±3.2950)	<b>160.3409</b> (±1.4917)	175.1557 (±2.0840)	255.9331 (±1.3856)
meps19 (15785, 139)	72.7294 (±1.8712)	72.3931 (±1.5869)	96.1294 (±1.7152)	<b>67.4596</b> (±1.6830)	<b>69.8709</b> (±1.5285)	<b>69.8846</b> (±1.6030)
superconductivity (21263, 81)	43.3530 (±0.7162)	43.6964 (±0.8383)	53.2923 (±0.7698)	<b>39.7680</b> (±0.4728)	<b>39.8094</b> (±0.4748)	47.4960 (±0.6617)
WEC (54007, 98)	89040.8808 (±1678.3201)	85806.8518 (±2294.9752)	111665.3580 (±2516.2890)	<b>71041.3455</b> (±1730.1204)	<b>69236.5148</b> (±1656.1975)	158154.4403 (±1452.0551)
kernel (241600, 15)	9.6111 (±0.0528)	8.0250 (±0.0477)	13.6089 (±0.0803)	<b>7.9097</b> (±0.0428)	8.5679 (±0.0557)	9.9090 (±0.0397)

Table 8: **Calibration Time.** The results are obtained over the specified iterations, with standard errors reported at the 95% confidence level. \*As NGB is a non-conformal method, it does not perform calibration; however, it provides prediction response values that can be used to estimate prediction intervals. (seconds)

Dataset	Type of method				
	Conformal				Non-conformal
	LoBoost	Locart	WICP	MICP	*NGB
airfoil (1503, 5)	0.0887 ( $\pm 0.0090$ )	<b>0.0103</b> ( $\pm 0.0005$ )	0.1351 ( $\pm 0.0133$ )	0.3708 ( $\pm 0.0036$ )	0.2199 ( $\pm 0.0024$ )
winered (1599, 11)	0.0251 ( $\pm 0.0039$ )	<b>0.0075</b> ( $\pm 0.0002$ )	0.1054 ( $\pm 0.0145$ )	0.7016 ( $\pm 0.0069$ )	0.2267 ( $\pm 0.0028$ )
star (2161, 39)	0.0247 ( $\pm 0.0032$ )	<b>0.0087</b> ( $\pm 0.0003$ )	0.1110 ( $\pm 0.0164$ )	1.5891 ( $\pm 0.0108$ )	0.2675 ( $\pm 0.0022$ )
winewhite (4898, 11)	0.0481 ( $\pm 0.0055$ )	<b>0.0166</b> ( $\pm 0.0007$ )	0.2500 ( $\pm 0.0324$ )	2.0492 ( $\pm 0.0189$ )	0.2766 ( $\pm 0.0035$ )
cycle (9568, 4)	0.1003 ( $\pm 0.0130$ )	<b>0.0354</b> ( $\pm 0.0024$ )	0.6910 ( $\pm 0.1090$ )	1.7081 ( $\pm 0.0056$ )	0.1734 ( $\pm 0.0012$ )
electric (10000, 12)	<b>0.0195</b> ( $\pm 0.0004$ )	0.0289 ( $\pm 0.0006$ )	0.3796 ( $\pm 0.0015$ )	4.6681 ( $\pm 0.0076$ )	0.2123 ( $\pm 0.0016$ )
bike (10886, 18)	0.2753 ( $\pm 0.0297$ )	<b>0.0934</b> ( $\pm 0.0060$ )	1.1954 ( $\pm 0.1293$ )	3.9485 ( $\pm 0.0144$ )	0.4285 ( $\pm 0.0029$ )
meps19 (15785, 139)	<b>0.0843</b> ( $\pm 0.0052$ )	0.1924 ( $\pm 0.0033$ )	2.1098 ( $\pm 0.3101$ )	14.7012 ( $\pm 0.0510$ )	0.7764 ( $\pm 0.0116$ )
superconductivity (21263, 81)	<b>0.1247</b> ( $\pm 0.0270$ )	0.2291 ( $\pm 0.0113$ )	15.7158 ( $\pm 3.5453$ )	24.1906 ( $\pm 0.7962$ )	0.2813 ( $\pm 0.0090$ )
WEC (54007, 98)	<b>0.4688</b> ( $\pm 0.0235$ )	0.9356 ( $\pm 0.0488$ )	44.5180 ( $\pm 8.7348$ )	27.9981 ( $\pm 0.3992$ )	0.9537 ( $\pm 0.1766$ )
kernel (241600, 15)	3.3821 ( $\pm 0.2022$ )	2.2344 ( $\pm 0.0385$ )	17.0551 ( $\pm 3.1195$ )	27.1017 ( $\pm 0.3944$ )	<b>1.0617</b> ( $\pm 0.0129$ )

Table 9: **MSE results.** Test MSE of the underlying point predictor, averaged over the specified iterations, with 95% confidence intervals. **LoBoost** and ICP share the same trained base predictor (hence the same MSE), while the remaining conformal baselines (Locart/WICP/MICP) also share a common base predictor and are grouped under *Other Methods*. NGB uses a different base model and is reported separately.

<b>Dataset</b>	<b>LoBoost</b>	<b>Other Methods</b>	<b>NGB</b>
airfoil (1503, 5)	<b>9.5760</b> (± <b>0.3352</b> )	12.1796 (±0.4536)	<b>9.7138</b> (± <b>0.2998</b> )
winered (1599, 11)	<b>0.4025</b> (± <b>0.0098</b> )	<b>0.4131</b> (± <b>0.0101</b> )	<b>0.4034</b> (± <b>0.0102</b> )
star (2161, 39)	<b>56192.8172</b> (± <b>918.6074</b> )	<b>56882.6099</b> (± <b>849.1448</b> )	<b>55944.5162</b> (± <b>832.2268</b> )
winewhite (4898, 11)	<b>0.4805</b> (± <b>0.0076</b> )	<b>0.4919</b> (± <b>0.0079</b> )	0.4987 (±0.0072)
cycle (9568, 4)	<b>13.0029</b> (± <b>0.3188</b> )	<b>13.4732</b> (± <b>0.2874</b> )	15.4420 (±0.2615)
electric (10000, 12)	<b>0.0002</b> (± <b>0.0000</b> )	0.0002 (±0.0000)	0.0002 (±0.0000)
bike (10886, 18)	<b>1907.7617</b> (± <b>44.2406</b> )	2023.8861 (±51.2551)	6981.8723 (±101.1801)
meps19 (15785, 139)	<b>584.4834</b> (± <b>31.1331</b> )	<b>585.4766</b> (± <b>31.2732</b> )	<b>601.2781</b> (± <b>31.3836</b> )
superconductivity (21263, 81)	<b>108.4250</b> (± <b>2.9847</b> )	<b>114.2662</b> (± <b>3.4007</b> )	170.7684 (±3.3283)
WEC (54007, 98)	<b>474917229.9098</b> (± <b>16829003.6959</b> )	<b>496520728.6553</b> (± <b>24823600.7984</b> )	1781811638.8855 (±33403412.6884)
kernel (241600, 15)	<b>9.4638</b> (± <b>0.1719</b> )	9.9576 (±0.1974)	11.7857 (±0.1465)

The low computational time compared to the other methods across different datasets—particularly in scenarios with large sample sizes and high-dimensional feature spaces—demonstrates the scalability of **LoBoost**.

Since **LoBoost** does not require retraining, it allows practitioners to focus on strengthening the underlying predictive boosting model while still obtaining reliable prediction intervals.

## D. Assumption 1 validation

To assess the geometric second-moment decay in Assumption 1, we run a synthetic one-dimensional heteroscedastic regression experiment (under two simulation settings). In each replication, we sample covariates independently as

$$X_i \stackrel{iid}{\sim} \text{Unif}[-2, 2], \quad i = 1, \dots, n,$$

and generate responses according to

$$Y_i = m(X_i) + \sigma(X_i) \varepsilon_i, \quad \varepsilon_i \stackrel{iid}{\sim} \mathcal{N}(0, 1),$$

where  $m(\cdot)$  and  $\sigma(\cdot)$  are simulation-specific mean and noise-scale functions. The sample is split into training, calibration, and test sets, and we fit LoBoost.

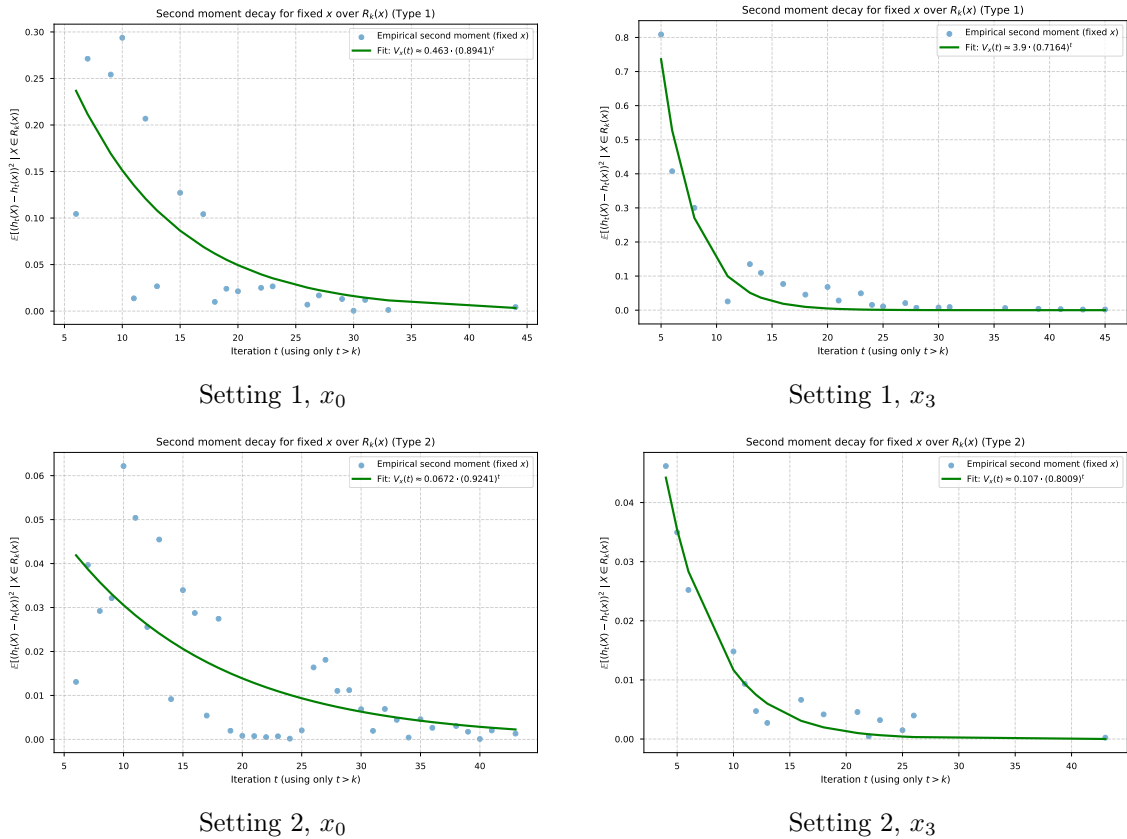


Figure 3: Empirical second-moment decay curves for fixed reference points  $x$  within boosting-induced regions  $\mathcal{R}_k(x)$  (here,  $k = 3$ ). The first row corresponds to simulation setting 1 and the second row to simulation setting 2. In each panel, we estimate  $\mathbb{E}[(h_t(X) - h_t(x))^2 | X \in \mathcal{R}_k(x)]$  empirically as a function of  $t$  and fit an exponential decay model  $V_x(t) \approx C\rho^t$ .

For a fixed depth  $k = 3$ , we form boosting-induced regions  $\mathcal{R}_k(\cdot)$  from the first  $k$  trees. To estimate the conditional second moment in Assumption 1, we fix a test point  $x$  and consider its associated region  $\mathcal{R}_k(x)$ . For each  $t > k$ , we estimate

$$\mathbb{E}[(h_t(X) - h_t(x))^2 | X \in \mathcal{R}_k(x)]$$

by the within-region sample average over test points in  $\mathcal{R}_k(x)$ , using the fitted  $t$ -th tree contribution  $h_t$  and the fixed reference value  $h_t(x)$ . Repeating this over  $t$  yields an empirical curve  $V_x(t)$ , to which we fit an exponential model

$$V_x(t) \approx C\rho^t.$$

The results are shown in Figure 3.

## E. Proofs of Theoretical Results

This appendix collects proofs of the main theoretical statements. Throughout, we exploit the additive structure of gradient boosting,  $g_T = \eta \sum_{t=1}^T h_t$ , together with the definition of the boosting-induced regions  $\mathcal{R}_k(x)$ : for any  $X \in \mathcal{R}_k(x)$ , the first  $k$  trees produce the same path/leaf as at  $x$ , so any discrepancy between  $g_T(X)$  and  $g_T(x)$  can only come from the “tail” of the ensemble (trees  $t > k$ ).

*Proof of Proposition 1.* Let  $X \sim_k x$ , then:

$$\begin{aligned} \mathbb{I}[X \sim_k x] (g_T(X) - g_T(x))^2 &= \mathbb{I}[X \sim_k x] \left( \eta \sum_{t>k}^T (h_t(X) - h_t(x)) \right)^2 \\ &= \eta^2 (T-k)^2 \mathbb{I}[X \sim_k x] \left( \frac{1}{T-k} \sum_{t>k}^T (h_t(X) - h_t(x)) \right)^2 \\ &\leq \eta^2 (T-k) \mathbb{I}[X \sim_k x] \sum_{t>k}^T (h_t(X) - h_t(x))^2 \end{aligned}$$

Take expectation over  $X$  in the previous inequality:

$$\mathbb{E} [(g_T(X) - g_T(x))^2 \mid X \in \mathcal{R}_k(x)] \leq \eta^2 (T-k) \sum_{t>k}^T \mathbb{E} [(h_t(X) - h_t(x))^2 \mid X \in \mathcal{R}_k(x)].$$

Applying Chebyshev’s inequality now gives

$$\begin{aligned} \mathbb{P} (|g_T(X) - g_T(x)| \geq \varepsilon \mid X \in \mathcal{R}_k(x)) &\leq \frac{1}{\varepsilon^2} \mathbb{E} [(g_T(X) - g_T(x))^2 \mid X \in \mathcal{R}_k(x)] \\ &\leq \frac{\eta^2 (T-k)}{\varepsilon^2} \sum_{t>k}^T \mathbb{E} [(h_t(X) - h_t(x))^2 \mid X \in \mathcal{R}_k(x)]. \end{aligned}$$

□

*Proof of Corollary 1.* By Proposition 1 and Assumption 1,

$$\begin{aligned} \mathbb{P} (|g_T(X) - g_T(x)| \geq \varepsilon \mid X \in \mathcal{R}_k(x)) &\leq \frac{\eta^2 (T-k)}{\varepsilon^2} \sum_{t=k+1}^T \mathbb{E} [(h_t(X) - h_t(x))^2 \mid X \in \mathcal{R}_k(x)] \\ &\leq \frac{C(x) \eta^2 (T-k)}{\varepsilon^2} \sum_{t=k+1}^T \rho^t. \end{aligned}$$

Summing the geometric series gives

$$\sum_{t=k+1}^T \rho^t = \rho^{k+1} \frac{1 - \rho^{T-k}}{1 - \rho} \leq \frac{\rho^{k+1}}{1 - \rho},$$

and therefore

$$\mathbb{P} (|g_T(X) - g_T(x)| \geq \varepsilon \mid X \in \mathcal{R}_k(x)) \leq \frac{C(x) \eta^2 (T-k)}{\varepsilon^2 (1 - \rho)} \rho^{k+1},$$

which is the first display in the corollary.  $\square$

*Proof of Corollary 2.* By Corollary 1 and the triangle inequality,

$$|s(X, Y) - s(x, Y)| \leq |g_T(X) - g_T(x)|,$$

we transform the probability over  $g$  to the probability over the residuals.

Next, fix  $\delta \in (0, 1)$ . Using the fact that  $T - K < T$ , we want to find  $k$  such that

$$\frac{C(x) \eta^2 T}{\varepsilon^2 (1 - \rho)} \rho^{k+1} \leq \delta.$$

Rearranging,

$$\rho^{k+1} \leq \delta \frac{\varepsilon^2 (1 - \rho)}{C(x) \eta^2 T}.$$

Taking logarithms yields

$$(k + 1) \log \rho \leq \log \left( \delta \frac{\varepsilon^2 (1 - \rho)}{C(x) \eta^2 T} \right).$$

Since  $\log \rho < 0$ , dividing by  $\log \rho$  reverses the inequality:

$$k + 1 \geq \frac{1}{-\log \rho} \log \left( \frac{C(x) \eta^2 T}{\delta \varepsilon^2 (1 - \rho)} \right),$$

i.e.,

$$k \geq \frac{1}{-\log \rho} \log \left( \frac{C(x) \eta^2 T}{\delta \varepsilon^2 (1 - \rho)} \right) - 1,$$

which is the stated sufficient condition.  $\square$

Before proving our main result, we collect a few regularity conditions used in the asymptotic analysis. The first one prevents the local regions induced by the partition from becoming asymptotically empty, ensuring that conditional probabilities of the form  $\mathbb{P}(\cdot | X \in \mathcal{R}_k(x))$  are well-defined in the regimes of interest.

**Assumption 2** (Well-populated partition). *Assume that the partition cells are uniformly well-populated: there exists a constant  $\gamma > 0$  such that, for every  $T$  and every  $k$  under consideration (in particular, for  $k = k(x, T, \varepsilon, \delta)$  as defined in Step 1),*

$$\mathbb{P}(X \in \mathcal{R}_k(x)) \geq \gamma.$$

Next, we require the local regions around  $x$  to shrink as the resolution increases.

**Assumption 3** (Shrinkage to  $x$ ). *For each fixed  $x \in \mathcal{X}$ , the regions satisfy*

$$\text{diam}(\mathcal{R}_k(x)) \xrightarrow[k \rightarrow \infty]{} 0.$$

Assumption 3 is purely geometric: for large  $k$ , membership in  $\mathcal{R}_k(x)$  forces  $X$  to be close to  $x$ . To translate this geometric shrinkage into convergence of conditional laws, we impose a mild smoothness condition on the conditional density.

**Assumption 4** (Locally Lipschitz conditional density on compacts). *Assume that for every compact set  $K \subset \mathbb{R}$  there exists a constant  $L_K < \infty$  such that, for all  $x, z \in \mathcal{X}$  and all  $y \in K$ ,*

$$|p(y | x) - p(y | z)| \leq L_K \|x - z\|.$$

Together, Assumptions 3 and 4 imply that conditioning on  $X \in \mathcal{R}_k(x)$  approximates conditioning on  $X = x$ : as  $k \rightarrow \infty$ , the conditional distribution of  $Y$  given  $X \in \mathcal{R}_k(x)$  converges to the conditional distribution of  $Y$  given  $X = x$ . Consequently, the corresponding population distribution of residuals inside  $\mathcal{R}_k(x)$  converges to the residual distribution at  $x$ .

Finally, to relate these population statements to the empirical conformal quantile, we track the number of calibration points that fall in  $\mathcal{R}_k(x)$ . Let  $\mathcal{D}_{\text{cal}} = \{(X_i, Y_i)\}_{i=1}^{n_{\text{cal}}}$  be the calibration sample and define

$$m_k(x) := \sum_{i=1}^{n_{\text{cal}}} \mathbb{I}[X_i \in \mathcal{R}_k(x)].$$

*Proof of Theorem 2.* Fix  $x \in \mathcal{X}$  and  $t \in \mathbb{R}$ . For notational convenience, define

$$S_X := |Y - g_T(X)|, \quad S_x := |Y - g_T(x)|.$$

**Step 0: Choosing  $\varepsilon, \delta$ .** Set  $\varepsilon_T := T^{-1/4}$  and

$$k := k(T) := \left\lceil \frac{2}{-\log \rho} \log T \right\rceil,$$

so that  $k \rightarrow \infty$  and  $k \in O(\log T)$  as  $T \rightarrow \infty$ . Define

$$\delta_T := C(x) \frac{\eta^2(T-k)}{\varepsilon_T^2} \frac{\rho^{k+1}}{1-\rho}.$$

We claim that  $\varepsilon_T \rightarrow 0$  and  $\delta_T \rightarrow 0$  as  $T \rightarrow \infty$ . The first claim is immediate. For the second, note that  $\varepsilon_T^2 = T^{-1/2}$ , hence

$$\frac{T-k}{\varepsilon_T^2} = (T-k) T^{1/2} \leq T \cdot T^{1/2} = T^{3/2},$$

where we used  $k \geq 0$ . Next, since  $\rho \in (0, 1)$  and  $k \geq \frac{2}{-\log \rho} \log T$ , we have

$$(k+1) \log \rho \leq \left( \frac{2}{-\log \rho} \log T + 1 \right) \log \rho = -2 \log T + \log \rho.$$

Exponentiating both sides yields

$$\rho^{k+1} = \exp((k+1) \log \rho) \leq \exp(-2 \log T + \log \rho) = \rho T^{-2}.$$

Combining the previous displays gives the explicit bound

$$\delta_T = C(x) \eta^2 \frac{T-k}{\varepsilon_T^2} \frac{\rho^{k+1}}{1-\rho} \leq C(x) \eta^2 T^{3/2} \frac{\rho T^{-2}}{1-\rho} = \frac{C(x) \eta^2 \rho}{1-\rho} T^{-1/2},$$

which converges to 0 as  $T \rightarrow \infty$ .

**Step 1: Residual continuity on a high-probability event.** By Corollary 2, there exists an event  $\Gamma := \Gamma_{x,T,\varepsilon_T,\delta_T,k} \subset \{\omega : X(\omega) \in \mathcal{R}_k(x)\}$  with

$$\mathbb{P}(\Gamma \mid X \in \mathcal{R}_k(x)) \geq 1 - \delta_T$$

such that, conditionally on  $\Gamma$  and  $X \in \mathcal{R}_k(x)$ ,

$$|S_X - S_x| \leq \varepsilon_T.$$

**Step 2: Upper bound.** Note that,

$$\begin{aligned} \mathbb{P}(S_X \leq t \mid X \in \mathcal{R}_k(x)) &= \mathbb{P}(S_X \leq t \mid \Gamma, X \in \mathcal{R}_k(x)) \mathbb{P}(\Gamma \mid X \in \mathcal{R}_k(x)) \\ &\quad + \mathbb{P}(S_X \leq t \mid \Gamma^C, X \in \mathcal{R}_k(x)) \mathbb{P}(\Gamma^C \mid X \in \mathcal{R}_k(x)) \\ &\leq \mathbb{P}(S_x \leq t + \varepsilon_T \mid \Gamma, X \in \mathcal{R}_k(x)) + \delta_T \\ &= \frac{\mathbb{P}(S_x \leq t + \varepsilon_T, \Gamma \mid X \in \mathcal{R}_k(x))}{\mathbb{P}(\Gamma \mid X \in \mathcal{R}_k(x))} + \delta_T \\ &\leq \frac{\mathbb{P}(S_x \leq t + \varepsilon_T \mid X \in \mathcal{R}_k(x))}{1 - \delta_T} + \delta_T. \end{aligned}$$

**Step 3: Lower bound.** Note that, on  $\Gamma$ ,  $S_x \leq t - \varepsilon_T$  implies  $S_X \leq t$ . Therefore, using the fact that  $\mathbb{P}(A \cap B) \geq \mathbb{P}(A) - \mathbb{P}(B^c)$ ,

$$\begin{aligned} \mathbb{P}(S_X \leq t \mid X \in \mathcal{R}_k(x)) &\geq \mathbb{P}(S_X \leq t \mid \Gamma, X \in \mathcal{R}_k(x)) \mathbb{P}(\Gamma \mid X \in \mathcal{R}_k(x)) \\ &\geq \mathbb{P}(S_x \leq t - \varepsilon_T \mid \Gamma, X \in \mathcal{R}_k(x)) \mathbb{P}(\Gamma \mid X \in \mathcal{R}_k(x)) \\ &= \mathbb{P}(S_x \leq t - \varepsilon_T, \Gamma \mid X \in \mathcal{R}_k(x)) \\ &\geq \mathbb{P}(S_x \leq t - \varepsilon_T \mid X \in \mathcal{R}_k(x)) - \mathbb{P}(\Gamma^C \mid X \in \mathcal{R}_k(x)) \\ &\geq \mathbb{P}(S_x \leq t - \varepsilon_T \mid X \in \mathcal{R}_k(x)) - \delta_T. \end{aligned}$$

Combining Steps 2–3 yields, for every  $t \in \mathbb{R}$ ,

$$\mathbb{P}(S_x \leq t - \varepsilon_T \mid X \in \mathcal{R}_k(x)) - \delta_T \leq \mathbb{P}(S_X \leq t \mid X \in \mathcal{R}_k(x)) \leq \frac{\mathbb{P}(S_x \leq t + \varepsilon_T \mid X \in \mathcal{R}_k(x))}{1 - \delta_T} + \delta_T. \quad (3)$$

**Step 4: Convergence of  $\mathbb{P}(S_x \leq s \mid X \in \mathcal{R}_k(x))$ .** Note that

$$\begin{aligned} \mathbb{P}(S_x \leq t \mid X \in \mathcal{R}_k(x)) &= \frac{1}{\mathbb{P}(X \in \mathcal{R}_k(x))} \int \int_{z \in \mathcal{R}_k(x)} \mathbb{I}[|y - g_T(x)| \leq t] p(z, y) dz dy \\ &= \int \mathbb{I}[|y - g_T(x)| \leq t] \left( \frac{1}{\mathbb{P}(X \in \mathcal{R}_k(x))} \int_{z \in \mathcal{R}_k(x)} p(y \mid z) p(z) dz \right) dy. \end{aligned}$$

Let

$$q_k(y) := \frac{1}{\mathbb{P}(X \in \mathcal{R}_k(x))} \int_{z \in \mathcal{R}_k(x)} p(y \mid z) p(z) dz.$$

By Assumption 4, for every compact set  $K \subset \mathbb{R}$  there exists  $L_K < \infty$  such that  $z \mapsto p(y \mid z)$  is  $L_K$ -Lipschitz uniformly over  $y \in K$ . Fix  $t \geq 0$  and let

$$K_t := [g_T(x) - t, g_T(x) + t],$$

which is compact. Then for every  $y \in K_t$ ,

$$|q_k(y) - p(y \mid x)| \leq \frac{1}{\mathbb{P}(X \in \mathcal{R}_k(x))} \int_{z \in \mathcal{R}_k(x)} |p(y \mid z) - p(y \mid x)| p(z) dz \leq L_{K_t} \text{diam}(\mathcal{R}_k(x)).$$

Therefore, for every  $t \geq 0$ ,

$$\begin{aligned} \left| \mathbb{P}(S_x \leq t \mid X \in \mathcal{R}_k(x)) - \mathbb{P}(S_x \leq t \mid X = x) \right| &= \left| \int \mathbb{I}[|y - g_T(x)| \leq t] (q_k(y) - p(y \mid x)) dy \right| \\ &\leq \int \mathbb{I}[|y - g_T(x)| \leq t] |q_k(y) - p(y \mid x)| dy \\ &\leq \int_{K_t} L_{K_t} \text{diam}(\mathcal{R}_k(x)) dy \\ &= 2t L_{K_t} \text{diam}(\mathcal{R}_k(x)), \end{aligned}$$

which converges to 0 as  $k \rightarrow \infty$ . Hence,

$$\lim_{k \rightarrow \infty} \mathbb{P}(S_x \leq t \mid X \in \mathcal{R}_k(x)) = \mathbb{P}(S_x \leq t \mid X = x).$$

Equivalently, the conditional distribution of  $S_x$  given  $X \in \mathcal{R}_k(x)$  converges weakly (in distribution) to the conditional distribution of  $S_x$  given  $X = x$  (van der Vaart, 1998, Lemma 2.2 (Portmanteau)).

**Step 5: Taking  $T \rightarrow \infty$ .** Since  $k = k(T) \rightarrow \infty$  as  $T \rightarrow \infty$ , Step 4 implies that for every  $u \in \mathbb{R}$ ,

$$\lim_{T \rightarrow \infty} \mathbb{P}(S_x \leq u \mid X \in \mathcal{R}_k(x)) = \mathbb{P}(S_x \leq u \mid X = x).$$

Applying  $\liminf_{T \rightarrow \infty}$  and  $\limsup_{T \rightarrow \infty}$  to (3) and using  $\delta_T \rightarrow 0$  yields

$$\begin{aligned} \mathbb{P}(S_x \leq t - \varepsilon_T \mid X = x) &\leq \liminf_{T \rightarrow \infty} \mathbb{P}(S_X \leq t \mid X \in \mathcal{R}_k(x)) \\ &\leq \limsup_{T \rightarrow \infty} \mathbb{P}(S_X \leq t \mid X \in \mathcal{R}_k(x)) \leq \mathbb{P}(S_x \leq t + \varepsilon_T \mid X = x). \end{aligned}$$

Finally, since  $\varepsilon_T \rightarrow 0$  and distribution functions are right-continuous, at every continuity point  $t$  of the conditional distribution of  $S_x$  given  $X = x$ ,

$$\lim_{T \rightarrow \infty} \mathbb{P}(S_X \leq t \mid X \in \mathcal{R}_k(x)) = \mathbb{P}(S_x \leq t \mid X = x) = \mathbb{P}(S_X \leq t \mid X = x).$$

**Step 6: Populational quantile convergence.** Define the distribution functions

$$F_k(s) := \mathbb{P}(S_X \leq s \mid X \in \mathcal{R}_k(x)), \quad F(s) := \mathbb{P}(S_x \leq s \mid X = x).$$

We have shown in Step 4 that  $F_k(s) \rightarrow F(s)$  at every continuity point of  $F$ , hence  $F_k \rightsquigarrow F$ . It is standard that weak convergence implies convergence of the corresponding quantiles at continuity points of the generalized inverse (van der Vaart, 1998, Lemma 21.2). For completeness, we provide the short argument below.

Let  $V \sim N(0, 1)$  be independent. Since  $F_k(v) \rightarrow F(v)$  for every continuity point  $v$  of  $F$ , and  $V$  has a continuous distribution, it follows that  $F_k(V) \rightarrow F(V)$  almost surely. Therefore  $F_k(V) \rightsquigarrow F(V)$  and, by the Portmanteau theorem,

$$\mathbb{P}(F_k(V) < u) \rightarrow \mathbb{P}(F(V) < u)$$

for every continuity point  $u$  of the distribution function of  $F(V)$ .

Using the generalized inverse identity  $\{F_k(V) < u\} \iff \{V < F_k^{-1}(u)\}$ , we obtain

$$\mathbb{P}(F_k(V) < u) = \mathbb{P}(V < F_k^{-1}(u)) = \Phi(F_k^{-1}(u)), \quad \mathbb{P}(F(V) < u) = \Phi(F^{-1}(u)),$$

where  $\Phi$  is the standard normal distribution function. Hence,  $\Phi(F_k^{-1}(u)) \rightarrow \Phi(F^{-1}(u))$  for every such  $u$ , and since  $\Phi$  is continuous and strictly increasing,

$$F_k^{-1}(u) \rightarrow F^{-1}(u)$$

at every continuity point  $u$  of  $F^{-1}$ . Taking  $u = 1 - \alpha$  yields  $q_{k,1-\alpha} \rightarrow q_{1-\alpha}$ , where  $q_{k,1-\alpha} := F_k^{-1}(1 - \alpha)$  and  $q_{1-\alpha} := F^{-1}(1 - \alpha)$ .

Assume that  $u = 1 - \alpha$  is a continuity point of  $F^{-1}$ , equivalently that  $F$  is continuous at  $q_{1-\alpha} := F^{-1}(1 - \alpha)$ . Let

$$q_{k,1-\alpha} := F_k^{-1}(1 - \alpha), \quad q_{1-\alpha} := F^{-1}(1 - \alpha).$$

Then  $q_{k,1-\alpha} \rightarrow q_{1-\alpha}$ .

It remains to pass from quantile convergence to convergence of the coverage probabilities. Fix  $\varepsilon > 0$ . For all sufficiently large  $k$ ,  $q_{1-\alpha} - \varepsilon \leq q_{k,1-\alpha} \leq q_{1-\alpha} + \varepsilon$ . Since  $F_k$  is nondecreasing, we obtain the sandwich bounds

$$F_k(q_{1-\alpha} - \varepsilon) \leq F_k(q_{k,1-\alpha}) \leq F_k(q_{1-\alpha} + \varepsilon).$$

Taking  $\liminf$  and  $\limsup$  and using Step 4 (pointwise convergence at fixed arguments),

we get

$$\liminf_{k \rightarrow \infty} F_k(q_{k,1-\alpha}) \geq F(q_{1-\alpha} - \varepsilon), \quad \limsup_{k \rightarrow \infty} F_k(q_{k,1-\alpha}) \leq F(q_{1-\alpha} + \varepsilon).$$

By continuity of  $F$  at  $q_{1-\alpha}$  and letting  $\varepsilon \downarrow 0$ , both bounds converge to  $F(q_{1-\alpha}) = 1 - \alpha$ , hence

$$F_k(q_{k,1-\alpha}) \rightarrow 1 - \alpha.$$

Recalling that  $F_k(s) = \mathbb{P}(S_X \leq s \mid X \in \mathcal{R}_k(x))$  and  $k = k(T)$  as in Step 0, we conclude that

$$\lim_{T \rightarrow \infty} \mathbb{P}(S_X \leq q_{k,1-\alpha} \mid X \in \mathcal{R}_k(x)) = \mathbb{P}(S_x \leq q_{1-\alpha} \mid X = x) = 1 - \alpha.$$

**Step 7: Empirical quantile convergence.** Let  $\mathcal{D}_{\text{cal}} = \{(X_i, Y_i)\}_{i=1}^{n_{\text{cal}}}$  be the calibration sample and, for a fixed  $k$ , set

$$m_k(x) := \sum_{i=1}^{n_{\text{cal}}} \mathbb{I}[X_i \in \mathcal{R}_k(x)].$$

By Assumption 2, along the sequence  $k = k(T)$  the number of calibration points inside  $\mathcal{R}_k(x)$  diverges, i.e.,  $m_{k(T)}(x) \rightarrow \infty$  in probability.

Consider the calibration residuals restricted to  $\mathcal{R}_k(x)$ ,

$$\{|Y_i - g_T(X_i)| : X_i \in \mathcal{R}_k(x)\},$$

and let  $\hat{q}_{k,1-\alpha}$  denote their empirical  $(1 - \alpha)$ -quantile (with the usual split-conformal convention). Conditionally on  $\{X_i \in \mathcal{R}_k(x)\}_{i=1}^{n_{\text{cal}}}$ , these residuals are i.i.d. with distribution function  $F_k$ , hence by the Glivenko–Cantelli theorem,

$$\sup_{s \in \mathbb{R}} \left| \hat{F}_k(s) - F_k(s) \right| \xrightarrow{m_k(x) \rightarrow \infty} 0 \quad \text{a.s.},$$

where  $\hat{F}_k$  is the empirical CDF based on the  $m_k(x)$  selected points. If  $F_k$  is continuous at  $q_{k,1-\alpha} := F_k^{-1}(1 - \alpha)$ , this implies

$$\hat{q}_{k,1-\alpha} \xrightarrow{m_k(x) \rightarrow \infty} q_{k,1-\alpha} \quad \text{a.s.}$$

Combining Steps 6–7 with the sandwich bound in (3) yields the desired asymptotic conditional coverage at  $x$ .

□